Generalized Spatial Regression with Differential Regularization

Matthieu Wilhelm[a] and Laura M. Sangalli [b*]

[*a] Institut de Statistique, Université de Neuchâtel, Bellevaux 51, 2000 Neuchâtel;

[b] MOX – Laboratorio di Modellistica e di Calcolo Scientifico, Politecnico di

Milano, Piazza Leonardo da Vinci 32, 20133 Milano, Italy;

April 20, 2016

Abstract

We aim at analyzing geostatistical and areal data observed over irregularly shaped spatial domains and having a distribution within the exponential family. We propose a generalized additive model that allows to account for spatially-varying covariate information. The model is fitted by maximizing a penalized log-likelihood function, with a roughness penalty term that involves a differential quantity of the spatial field, computed over the domain of interest. Efficient estimation of the spatial field is achieved resorting to the finite element method, which provides a basis for piecewise polynomial surfaces. The proposed model is illustrated by an application to the study of criminality in the city of Portland, Oregon, USA.

Key words. Functional data analysis, spatial data analysis, generalized additive model, differential regularizations, finite element method.

1   Introduction and motivation

We propose a generalized regression model for spatially distributed data, when the response variable has a distribution within the exponential family. One of the main features of the model is that it is able to deal with domains having complex shapes, characterized for instance by strong concavities or holes, and where the shape of the domain influences the behavior of the phenomenon. To illustrate this problem, we consider the study of criminality

---

[**]Corresponding author. Email: laura.sangalli@polimi.it

over the city of Portland, Oregon, USA. The left panel of Figure 1 shows a map of this city, cut in two parts by the Willamette river. The two parts of the city are connected only by a few bridges. The dots over the map indicates the locations of all the crimes reported in 2012. It is apparent that the variation of the phenomenon is not smooth across the river. The map also shows the municipality districts. Census information is available for each district, such as the total number of residents per district. We would like to study the spatially-varying criminality in the city, taking into account the auxiliary information based on the census. Since the covariate is available at the level of districts, we aggregate also the crimes, thus considering as outcome of interest the total crime count over each districts.

When analyzing these data, it appears crucial to accurately take into account the shape of the domain. Features such as the river and the bridges in fact influence the phenomenon expression; see, e.g., Chainey and Ratcliffe [2005], Ratcliffe [2010]. See also Bernasco and Elffers [2010] for a comprehensive review on the statistical analysis of spatial crime data. Moreover, not restricted to criminology applications, there is a vast literature devoted to the study of spatially varying data having a distribution within the exponential family [see, e.g., Diggle and Ribeiro, 2007, and references therein]. However, these methods are not well suited for the analysis of the data here presented, as they do not account for the complex shape of the problem domain, neglecting for instance natural barriers such as the river.

Recently, some spatial data analysis methods have been proposed where the shape of the domain is directly specified in the model; these include the spatial regression models with differential regularization proposed in Ramsay [2002] and Sangalli et al. [2013], and the soap film smoothing introduced by Wood et al. [2008]. Here we propose an extension of the methodology presented in Sangalli et al. [2013], allowing to model response variables having a distribution within the exponential family, including binomial, gamma and Poisson outcomes. Specifically, we maximize a penalized log-likelihood function with a roughness penalty term that involves a differential quantity of the spatial field computed over the domain of interest. We name the resulting method GSR-PDE: Generalized Spatial Regression with PDE penalization. To solve the estimation problem, we derive a functional version of the Penalized Iterative Reweighted Least Squares (PIRLS) algorithm [O'Sullivan et al., 1986]. This functional version of the PIRLS algorithm can be used to maximize penalized log-likelihoods with general quadratic penalties involving a functional parameter. Likewise Ramsay [2002] and Sangalli et al. [2013], the proposed models make use of finite elements over a triangulation of the domain of interest, to obtain accurate estimates of the spatial field. See Ramsay [2000] for an earlier use of finite elements in a spatial data analysis context, and Lindgren et al. [2011] for the purpose of fitting Gaussian random fields. Domain triangulations are able to efficiently describe domains with complex geometries. The right panel of Figure 1 shows a triangulation

2

of the city of Portland. The triangulation accurately renders the strong concavities in the domain represented by the river, and also very localized and detailed structures of the domain such as the bridges that connect the two parts of the city center. The proposed model is detailed both for the case of geostatistical data and for the case of areal data. The model versions for geostatistical and for areal data are special cases of a unique model, although for simplicity of exposition we introduce first the version for geostatistical data, then the one for areal data, and we postpone to the appendix the unified modelling formulation. Some comparative simulation studies show the good performances of the model.

The paper is organized as follows. In section 2, we introduce the model, detailed in the case of geostatistical data. In the section 3, we derive the functional version of the PIRLS algorithm. In section 4, we describe the numerical implementation of the fitting procedure. In Section 5 we specify the model version for areal data. Section 6 is devoted to simulation studies and Section 7 to the study of criminality over the city of Portland. Finally, Section 8 draws some directions for future research. All technical details and proofs are deferred to the Appendix.
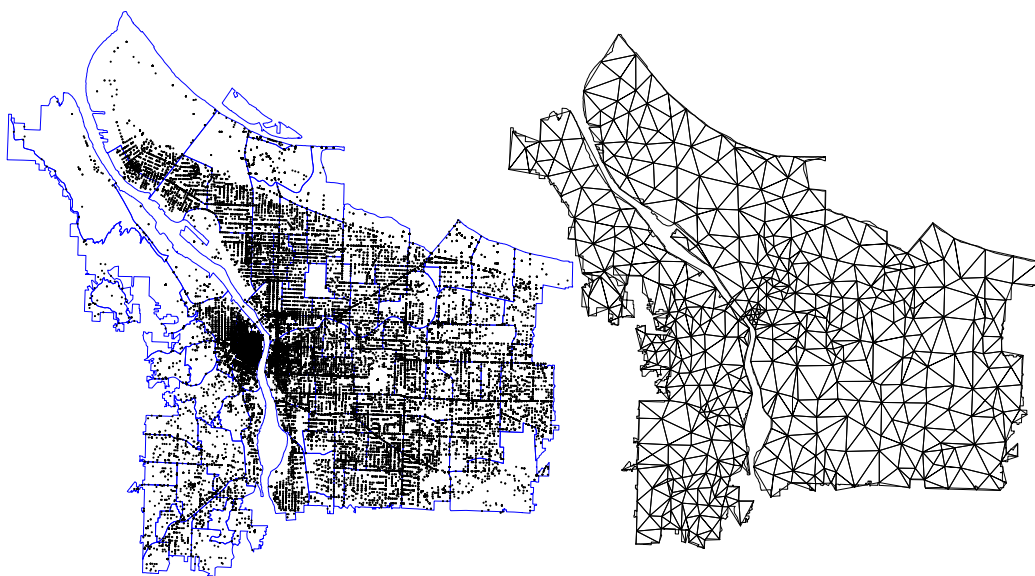

Figure 1: Left: crime locations in the city of Portland, Oregon, in 2012. Right: the triangulation of the domain, with the borders of the city districts highlighted in blue. In the data analysis, crimes are aggregated over districts, leading to the total crime counts shown in the left panel of Figure 9.

2 Model version for geostatistical data

We consider a bounded domain $\Omega \subset \mathbb{R}^2$ with a regular boundary $\partial\Omega \in C^2(\mathbb{R}^2)$. We consider n fixed locations $\mathbf{p}_1, \ldots, \mathbf{p}_n \in \Omega$, where $\mathbf{p}_i = (p_{1i}, p_{2i})$. At each $\mathbf{p}_i$ we observe the realization y_i of a real variable of interest Y_i, and a vector of covariate information $\mathbf{x}_i \in \mathbb{R}^q$. We assume $Y_1, \ldots, Y_n$ are independent, with Y_i having a distribution within the exponential family, with mean μ_i and common scale paramenter ϕ. We model μ_i by the following generalized additive model:

$$g(\mu_i) = \theta_i = x_i^t \boldsymbol{\beta} + f(\mathbf{p}_i), \tag{2.1}$$

where g is a continuously differentiable and strictly monotone canonical link function, $\boldsymbol{\beta} \in \mathbb{R}^q$ is a vector of coefficients, and f is a smooth field over Ω, lying in a suitable functional space $\mathcal{F}$. The parameter θ is referred to as the canonical parameter.

We then propose to estimate the regression coefficients $\boldsymbol{\beta} \in \mathbb{R}^q$ and the spatial field $f \in \mathcal{F}$ by maximizing a penalized log-likelihood functional:

$$\mathcal{L}_p(\boldsymbol{\beta}, f) = \sum_{i=1}^{n} l(y_i; \theta_i(\boldsymbol{\beta}, f)) - \lambda \int_\Omega \left(\Delta f(\mathbf{p}) \right)^2 d\mathbf{p}, \tag{2.2}$$

where $l(\cdot)$ is the log-likelihood and $\theta_i(\boldsymbol{\beta}, f) = \mathbf{x}_i^t \boldsymbol{\beta} + f(\mathbf{p}_i)$. Here λ is a positive smoothing parameter and the Laplacian $\Delta f = \partial^2 f / \partial p_1^2 + \partial^2 f / \partial p_2^2$ is a measure of the local curvature of the field f. The higher λ is, the more we control the wiggliness of the spatial field f, the smaller λ is, the more we allow flexibility of f. As discussed in Section 8, more complex roughness penalties may be considered. Azzimonti et al. [2014, 2015] for instance show that by changing the regularizing terms and considering more complex differential operators it is possible to include in the model a priori information about the spatial variation of the phenomenon under study, and model also space anisotropies and non-stationarities. As commented in Appendix A, the regularizing term in (2.2) effectively induces the spatial variation structure of the estimator and different regularizations imply different variation structures.

In the case of Gaussian observations, with mean $\mu_i = \theta_i$ and constant variance σ^2, the maximization of the penalized log-likelihood function is equivalent to the minimization of the penalized least-square functional considered in Sangalli et al. [2013]. In this case, the quadratic form of the functional allows to characterize analytically the minimum of the penalized least square functional (or equivalently, the maximum of the penalized log-likelihood functional), and thus to characterize the estimators $\hat{\boldsymbol{\beta}} \in \mathbb{R}^q$ and $\hat{f} \in \mathcal{F}$. Outside of the Gaussian case, it is not possible to characterize analytically the solution of the estimation problem. On the other hand, we cannot either apply the standard PIRLS algorithm, developed by O'Sullivan et al.

4

[1986] for the maximization of a penalized log-likelihood functional in the context of generalized additive models. This is due to the fact that the penalized log-likelihood in (2.2) involves a function parameter, the spatial field f, and the maximization is over the space $\mathbb{R}^q \times \mathcal{F}$, where $\mathcal{F}$ is an infinite-dimensional space. In the following section, we thus present a functional version of the PIRLS algorithm, that can be used to find an approximate solution of the estimation problem here considered. More generally, the proposed functional version of the PIRLS algorithm can be employed in the context of generalized linear models with a functional parameter, to maximize a penalized log-likelihood that has a quadratic penalty on the functional parameter.

3 Functional version of the PIRLS algorithm

We consider the following parametrization of a distribution from the exponential family:

$$f_Y(y; \theta, \phi) = \exp\left\{(y\theta - b(\theta))/a(\phi) + c(\phi, y)\right\},$$

where $a(\cdot)$, $b(\cdot)$ and $c(\cdot)$ are functions subject to some regularity constraints [see, e.g., McCullagh and Nelder, 1989]. For sake of simplicity, we only consider canonical link functions, that is $b'(\theta) = g^{-1}(\theta)$, and we make no distinction between the natural and the canonical parameter. Moreover, we assume that $a(\phi) = \phi$, this being the case of the most common distributions in the exponential family, including the Gaussian, gamma, binomial and Poisson distributions. We denote by $V(\cdot)$ the function satisfying $\mathrm{var}(Y) = V(\mu)\phi$.

In our case, the canonical parameter θ is a function of both $\boldsymbol{\beta} \in \mathbb{R}^q$ and $f \in \mathcal{F}$. We consider the more general penalized log-likelihood

$$\mathcal{L}_p(\boldsymbol{\beta}, f) = \mathcal{L}(\boldsymbol{\beta}, f) - \frac{\lambda}{2}\, m(f, f), \tag{3.1}$$

where $\mathcal{L}$ is the log-likelihood and $m(\cdot, \cdot) : \mathcal{F} \times \mathcal{F} \to \mathbb{R}$ is any bilinear, symmetric and semi-positive definite form. This allows us to introduce the functional version of the PIRLS algorithm for any functional roughness penalty of this general quadratic form.

We here give a sketch of the derivation of the algorithm and refer to Appendix B for all technical details. For simplicity of writing, we introduce a matrix notation: $\mathbf{y} = (y_1, \ldots, y_n)^t$ is the vector of observed data values, $\boldsymbol{\mu} = (\mu_1, \ldots, \mu_n)^t$ is the mean vector, $\mathbf{X} \in \mathbb{R}^{n \times q}$ denotes the design matrix, whose i-th row is given by the covariates $\mathbf{x}_i$ associated to y_i, $\mathbf{f}_n = (f(\mathbf{p}_1), \ldots, f(\mathbf{p}_n))^t$ is the vector of evaluations of the spatial field f at the n spatial locations and finally $\mathbf{V}$ is a $n \times n$ diagonal matrix with entries $V(\mu_1), \ldots, V(\mu_n)$, where $V(\cdot)$ is the variance function.

First, we show that the problem of maximizing (3.1) with respect to $(\boldsymbol{\beta}, f)$ is equivalent to minimizing the following functional $\mathcal{J}_\lambda(\boldsymbol{\beta}, f)$ with respect to $(\boldsymbol{\beta}, f)$:

$$\mathcal{J}_\lambda(\boldsymbol{\beta}, f) = \|\mathbf{V}^{-1/2}(\mathbf{y} - \boldsymbol{\mu}(\boldsymbol{\beta}, f))\|^2 + \lambda \, m(f, f),$$

where $\mathbf{V}$ is considered as fixed, and $\boldsymbol{\mu}(\boldsymbol{\beta}, f)$ is given by the equation (2.1). Since $\mathbf{V}$ in reality depends on $\boldsymbol{\beta}$ and f, this suggests an iterative scheme for the solution of the estimation problem. Let $\boldsymbol{\mu}^{(k)}$ be an estimate of $\boldsymbol{\mu}(\boldsymbol{\beta}, f)$ after k iterations of the algorithm, and let us consider a first order development of $\boldsymbol{\mu}(\boldsymbol{\beta}, f)$ in the neighborhood of the current value $\boldsymbol{\mu}^{(k)} = \boldsymbol{\mu}(\boldsymbol{\beta}^{(k)}, f^{(k)})$. We need to introduce the following notation: $\mathbf{z}^{(k)}$ is the current pseudo-data, defined by $\mathbf{z}^{(k)} = \mathbf{G}^{(k)}(\mathbf{y} - \boldsymbol{\mu}^{(k)}) + \boldsymbol{\theta}^{(k)}$, where $\boldsymbol{\theta}^{(k)}$ is the vector with entries $g(\mu_1^{(k)}), \ldots, g(\mu_n^{(k)})$ and $\mathbf{G}^{(k)}$ is the $n \times n$ diagonal matrix with entries $g'(\mu_1^{(k)}), \ldots, g'(\mu_n^{(k)})$; moreover, $\mathbf{V}^{(k)}$ is the current value of $\mathbf{V}$ for $\boldsymbol{\mu} = \boldsymbol{\mu}^{(k)}$ and $\mathbf{W}^{(k)} = (\mathbf{G}^{(k)})^{-2}(\mathbf{V}^{(k)})^{-1}$. The first order development of $\boldsymbol{\mu}(\boldsymbol{\beta}, f)$ in the neighborhood of the current value $\boldsymbol{\mu}^{(k)}$ is to be considered in the space $\mathbb{R}^q \times \mathcal{F}$ and yields the following quadratic approximation of $\mathcal{J}_\lambda(\boldsymbol{\beta}, f)$:

$$\tilde{\mathcal{J}}_\lambda^{(k)}(\boldsymbol{\beta}, f) = \|(\mathbf{W}^{(k)})^{1/2}(\mathbf{z}^{(k)} - \mathbf{X}\boldsymbol{\beta} - \mathbf{f}_n)\|^2 + \lambda \, m(f, f), \qquad (3.2)$$

We may thus consider the following iterative scheme. Let $\boldsymbol{\mu}^{(k)}$ be the value of $\boldsymbol{\mu}$ after k iterations of the algorithm. At the $k + 1$ iteration, the following steps are performed:

1. compute $\mathbf{z}^{(k)}$ and $\mathbf{W}^{(k)}$;

2. find $\boldsymbol{\beta}^{(k+1)}$ and $f^{(k+1)}$ that jointly minimize (3.2);

3. set $\boldsymbol{\mu}^{(k+1)} = g^{-1}(\mathbf{X}\boldsymbol{\beta}^{(k+1)} + \mathbf{f}_n^{(k+1)})$.

The stopping criterion is based on a sufficiently small variation of two successive values of the functional (3.2). The starting value $\boldsymbol{\mu}^0$ is set to $\mathbf{y}$. In the case of binary outcomes, $\boldsymbol{\mu}^0$ is set to $\boldsymbol{\mu}^0 = \frac{1}{2}(\mathbf{y} + \frac{1}{2})$.

When a canonical parameter is used, the log-likelihood of an exponential family distribution is strictly concave. Since the penalization term is concave too, the maximum of the penalized log-likelihood is unique, when it exists. Therefore, if the convergence of the functional PIRLS algorithm is reached, it always results in the maximum penalized log-likelihood estimate. In the simulations and application shown in this paper, just a very few iterations (less than 10) of the algorithm were sufficient to reach convergence, as it is usually the case for generalized linear models.

Step 2 of the algorithm still involves a minimization problem over an infinite dimensional space. In the case where the penalty has the form $m(f, f) = \int_\Omega \left(\Delta f(\mathbf{p})\right)^2 d\mathbf{p}$, this minimization problem can be solved extending the methodology described in Sangalli et al. [2013]. This extension will

6

be the object of the next section. However, the functional version of the PIRLS algorithm applies more generally to any type of quadratic roughness penalty.

4   Penalized least-square problem and finite elements

We now focus on the case where the roughness penalty has the form $m(f, f) = \int_\Omega \left(\Delta f(\mathbf{p}) \right)^2 d\mathbf{p}$. At each iteration of the functional PIRLS algorithm, we thus have to find the values of $\boldsymbol{\beta} \in \mathbb{R}^q$ and $f \in \mathcal{F}$ that jointly minimize

$$\tilde{\mathcal{J}}_\lambda \left(\boldsymbol{\beta}, f \right) = \| (\mathbf{W}^{1/2} (\mathbf{z} - \mathbf{X}\boldsymbol{\beta} - \mathbf{f}_n) \|^2 + \lambda \int_\Omega (\Delta f)^2. \qquad (4.1)$$

To simplify the notation we drop here and in the following the dependence on k, the iteration counter. Let us then consider what kind of space $\mathcal{F}$ is well-suited for the problem here considered. To do this, we need to introduce the Sobolev space $H^m(\Omega)$: this is the Hilbert space of all functions which belong to $L^2(\Omega)$ along with all their distributional derivatives up to the order m. Since the roughness penalty term $\int_\Omega (\Delta f)^2$ must be well defined, we need $\mathcal{F} \subset H^2(\Omega)$. Note that by the Sobolev embedding theorem, $H^2(\Omega) \subset C^0(\Omega)$. Thus, a function $f \in H^2(\Omega)$ is continuous and can hence be evaluated at pointwise locations, so that it is possible to compute the vector $\mathbf{f}_n$ in the least-square term (or in the log-likelihood). Moreover, to ensure uniqueness of the minimizer of (4.1), suitable boundary conditions are required. Boundary conditions are a way to impose a desired behaviour to the estimated function f at the boundaries of the domain of interest. Typically, we can impose conditions on the value of f at the boundary $\partial \Omega$, that is $f|_{\partial \Omega} = \gamma_D$ (*Dirichlet* type boundary conditions), or on the flux of the function through the boundary, that is $\partial_{\mathbf{n}} f|_{\partial \Omega} = (\nabla f)^t \mathbf{n} = \gamma_N$ (*Neumann* type boundary conditions), where $\mathbf{n}$ denotes the outward-pointing normal unit vector to the boundary and $\nabla f = (\partial f / \partial p_1, \partial f / \partial p_2)^t$ is the gradient of the function f. When the functions γ_D or γ_N coincide with null functions, the condition is said homogeneous. Moreover, it is possible to impose different boundary conditions on different portions of the boundary, forming a partition of $\partial \Omega$. To ensure the uniqueness of the minimization problem (4.1), we here consider the space:

$$\mathcal{F} = H^2_{\mathbf{n}_0} = \left\{ f \in H^2 \mid (\nabla f)^t \mathbf{n} = 0 \text{ on } \partial \Omega \right\}.$$

The interested reader is referred to Azzimonti et al. [2014, 2015] for the case of general boundary conditions.

4.1 Characterization of the solution to the penalized least-square problem

In the following, we assume that the design matrix $\mathbf{X}$ has full rank and that the weight matrix $\mathbf{W}$ has strictly positive entries. Let $\mathbf{H} = \mathbf{X}(\mathbf{X}^t\mathbf{W}\mathbf{X})^{-1}\mathbf{X}^t\mathbf{W}$, and $\mathbf{Q} = \mathbf{I}-\mathbf{H}$, where $\mathbf{I}$ is an identity matrix of appropriate dimension. Moreover, for any function u in the considered functional space $\mathcal{F} = H^2_{\mathbf{n}_0}(\Omega)$, we denote by $\mathbf{u}_n = u(\mathbf{p}_1),\ldots,u(\mathbf{p}_n)$ the vector of evaluations of u at the n spatial locations. Finally, we denote by $\tilde{\boldsymbol{\beta}}$ and $\tilde{f}$ the minimizers of the penalized least-square functional $\tilde{\mathcal{J}}_\lambda(\boldsymbol{\beta}, f)$ in (4.1), and by $\hat{\boldsymbol{\beta}}$ and $\hat{f}$ the maximizers of the penalized log-likelihood functional $\mathcal{L}_p(\boldsymbol{\beta}, f)$ in (2.2). Under these assumptions, the following Proposition characterizes the minimizers $\tilde{\boldsymbol{\beta}}$ and $\tilde{f}$ of the penalized least-square functional (4.1).

Proposition 4.1. *There exists a unique pair $(\tilde{\boldsymbol{\beta}}, \tilde{f}) \in \mathbb{R}^q \times H^2_{\mathbf{n}_0}$ which minimizes (4.1). Moreover,*

- $\tilde{\boldsymbol{\beta}} = (\mathbf{X}^t\mathbf{W}\mathbf{X})^{-1}\mathbf{X}^t\mathbf{W}(\mathbf{z} - \tilde{\mathbf{f}}_n)$, *where* $\tilde{\mathbf{f}}_n = (\tilde{f}(\mathbf{p}_1),\ldots,\tilde{f}(\mathbf{p}_n))^t$,

- $\tilde{f}$ *satisfies:*

$$\mathbf{u}_n^t\mathbf{Q}\,\tilde{\mathbf{f}}_n + \lambda \int_\Omega (\Delta u)(\Delta \tilde{f}) = \mathbf{u}_n^t\mathbf{Q}\,\mathbf{z}, \qquad \forall u \in H^2_{\mathbf{n}_0}. \qquad (4.2)$$

Proof. See appendix C. $\qquad\qquad\square$

Using Proposition 4.1 and the functional version of the PIRLS algorithm presented in Section 3, we have a characterization of the maximum penalized log-likelihood in the functional space $H^2_{\mathbf{n}_0}(\Omega)$.

4.2 Solution to the penalized least-square problem

In this section, we describe the methodology yielding to the solution of the problem of minimizing $\tilde{\mathcal{J}}_\lambda(\boldsymbol{\beta}, f)$ with respect to both $\boldsymbol{\beta}$ and f. As stated by the proposition 4.1, given $\tilde{f}$, it is easy to compute $\tilde{\boldsymbol{\beta}}$. Then, the crucial point is to find $\tilde{f}$ that satisfies (4.2). For this purpose, we introduce the space:

$$H^1_{\mathbf{n}_0} = \left\{ f \in H^1 \mid (\nabla f)^t\mathbf{n} = 0 \text{ on } \partial\Omega \right\}.$$

Then, as shown in Sangalli et al. [2013], problem (4.2) is equivalent to finding $(\tilde{f}, \tilde{h}) \in H^1_{\mathbf{n}_0}(\Omega) \times H^1_{\mathbf{n}_0}(\Omega)$ such that

$$\begin{cases} \mathbf{u}_n^t\mathbf{Q}\,\tilde{\mathbf{f}}_n - \lambda \int_\Omega (\nabla u)^t\nabla\tilde{h} = \mathbf{u}_n^t\mathbf{Q}\,\mathbf{z} \\[2mm] -\int_\Omega (\nabla\tilde{f})^t\nabla v = \int_\Omega \tilde{h}\,v. \end{cases} \qquad (4.3)$$

for any $(u, v) \in H^1_{\mathbf{n}_0} \times H^1_{\mathbf{n}_0}(\Omega)$. This formulation requires less regularity on the functions involved with respect to formulation (4.2), defined in $H^2_{\mathbf{n}_0}(\Omega)$. In the following section, we show how we can use the finite element method to construct a finite dimensional subspace of $H^1_{\mathbf{n}_0}(\Omega)$, and hence to compute an approximate solution to (4.3) in such space.

4.3 Finite elements

The finite element method is widely used in engineering applications to numerically solve problems involving partial differential equations [see, e.g., Quarteroni, 2014].

To construct a finite element space, we start by partitioning the domain of interest Ω into small subdomains. Convenient domain partitions are given for instance by triangular meshes. Figure 1, right panel, shows for example a triangulation of the domain of interest for the study of criminality in the city of Portland. We consider a regular triangulation $\mathcal{T}$ of Ω, where adjacent triangles share either a vertex or a complete edge. The domain Ω is hence approximated by the domain $\Omega_{\mathcal{T}}$ consisting of the union of all triangles, so that the boundary $\partial\Omega$ of Ω is approximated by a polygon (or more polygons, in the case for instance of domains with interior holes). The triangulation is able to describe accurately the complex domain geometry, with its strong concavities corresponding to the river and detailed local structures such as the bridges that connect the two sides of the city center.

Starting from the triangulation, locally supported polynomial functions are defined over the triangles, providing a set of basis functions $\psi_1, \ldots, \psi_K$, that span a finite dimensional subspace $\mathcal{F}_K$ of $H^1_{\mathbf{n}_0}$. Linear finite elements are for instance obtained considering a basis system where each basis function ψ_i is associated with a vertex $\boldsymbol{\xi}_i, i = 1, \ldots, K$, of the triangulation $\mathcal{T}$. This basis function ψ_i is a piecewise linear polynomial which takes the value one at the vertex $\boldsymbol{\xi}_i$ and the value zero on all the other vertices of the mesh, i.e., $\psi_i(\boldsymbol{\xi}_j) = \delta_{ij}$, for all $i, j = 1, \ldots, K$, where δ_{ij} denotes the Kronecker symbol. Figure 2 shows an example of such linear finite element basis function on a planar mesh, highlighting the locally supported nature of the basis.

Now, let $\boldsymbol{\psi} = (\psi_1, \ldots, \psi_K)^t$ be the column vector collecting the K piecewise linear basis functions associated with the K vertices $\boldsymbol{\xi}_1, \ldots, \boldsymbol{\xi}_K$. Each function h in the finite element space $\mathcal{F}_K$ can be represented as an expansion in terms of the basis functions $\psi_1, \ldots, \psi_K$. Let $\mathbf{h} = (h_1, \ldots, h_K)$ be the coefficients of the basis expansion of h, that is the coefficients such that

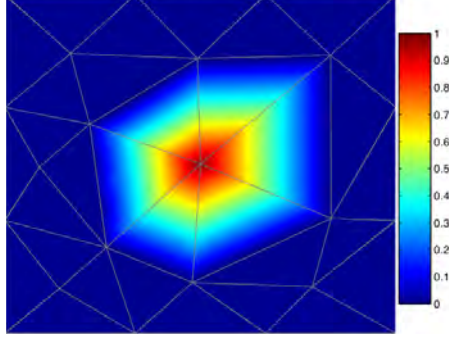$$h(\cdot) = \sum_{j=1}^{K} h_j \psi_j(\cdot) = \mathbf{h}^t \boldsymbol{\psi}(\cdot).$$

9

Figure 2: Linear finite element basis function.

Note that

$$h(\boldsymbol{\xi}_i) = \sum_{j=1}^{K} h_j \psi_j(\boldsymbol{\xi}_i) = \sum_{j=1}^{K} h_j \delta_{ij} = h_i,$$

hence

$$\mathbf{h} = \big(h(\boldsymbol{\xi}_1), \ldots, h(\boldsymbol{\xi}_K)\big),$$

which exhibits the fact that each function $h \in \mathcal{F}_K$ is fully characterized by its evaluations on the mesh nodes.

4.4 Numerical solution to the penalized least-square problem

The functions and integrals in (4.3) can be approximated using functions in the finite element space $\mathcal{F}_K$, so that problem (4.3) is approximated with its discrete counterpart: find $(\tilde{f}, \tilde{h}) \in \mathcal{F}_K \times \mathcal{F}_K$ that satisfy (4.3) for any $(u, v) \in \mathcal{F}_K \times \mathcal{F}_K$, where the integrals are now computed over the triangulation $\Omega_\mathcal{T}$. Let $\boldsymbol{\Psi}$ be the $n \times K$ matrix of the evaluations of the K basis at the n data locations $\mathbf{p}_1, \ldots, \mathbf{p}_n$,

$$\boldsymbol{\Psi} = \begin{bmatrix} \boldsymbol{\psi}^t(\mathbf{p}_1) \\ \vdots \\ \boldsymbol{\psi}^t(\mathbf{p}_n) \end{bmatrix} \tag{4.4}$$

and consider the $K \times K$ matrices

$$\mathbf{R_0} = \int_{\Omega_\mathcal{T}} (\boldsymbol{\psi} \ \boldsymbol{\psi}^t) \qquad \mathbf{R_1} = \int_{\Omega_\mathcal{T}} (\nabla \boldsymbol{\psi})^t \nabla \boldsymbol{\psi}.$$

Using this notation, for functions $\tilde{f}, \tilde{h}, u, v \in \mathcal{F}_K$, we can write the integrals in (4.3) as follows:

$$\int_{\Omega_\mathcal{T}} (\nabla u)^t \nabla \tilde{h} = \mathbf{u}^t \mathbf{R}_1 \tilde{\mathbf{h}}, \qquad \int_{\Omega_\mathcal{T}} (\nabla \tilde{f})^t \nabla v = \tilde{\mathbf{f}}^t \mathbf{R}_1 \mathbf{v}, \qquad \int_{\Omega_\mathcal{T}} \tilde{h} \ v = \tilde{\mathbf{h}}^t \mathbf{R}_0 \mathbf{v},$$

10

where $\tilde{\mathbf{f}}, \tilde{\mathbf{h}}, \mathbf{u}$ and $\mathbf{v}$ are the vectors of the basis expansions of the functions $\tilde{f}, \tilde{h}, u$ and v respectively. The discrete counterpart of the problem (4.3) thus reduces to solving a linear system, as stated in the following proposition.

Proposition 4.2. *The discrete counterpart of (4.3) is given by the system*

$$\begin{bmatrix} -\boldsymbol{\Psi}^t \ \mathbf{Q} \ \boldsymbol{\Psi} & \lambda \mathbf{R}_1 \\ \lambda \mathbf{R}_1 & \lambda \mathbf{R}_0 \end{bmatrix} \begin{bmatrix} \tilde{\mathbf{f}} \\ \tilde{\mathbf{h}} \end{bmatrix} = \begin{bmatrix} -\boldsymbol{\Psi}^t \mathbf{Q} \ \mathbf{z} \\ \mathbf{0} \end{bmatrix}, \qquad (4.5)$$

which admits a unique pair of solutions $\tilde{\mathbf{f}}, \tilde{\mathbf{h}}$ that are respectively the coefficients of the basis expansion of $\tilde{f}$ and $\tilde{h}$.

Proof. Uniqueness of the solution to (4.5) is ensured by the positive definiteness of the matrices $\mathbf{R}_0$ and $\left(\boldsymbol{\Psi}^t \mathbf{Q} \boldsymbol{\Psi} + \lambda \mathbf{R}_1 \mathbf{R}_0^{-1} \mathbf{R}_1 \right)$. $\qquad\square$

Let $\boldsymbol{P} = \mathbf{R}_1 \mathbf{R}_0^{-1} \mathbf{R}_1$ and $\mathbf{S} = \boldsymbol{\Psi} \left(\boldsymbol{\Psi}^t \ \mathbf{Q} \ \boldsymbol{\Psi} + \lambda \boldsymbol{P} \right)^{-1} \boldsymbol{\Psi}^t \mathbf{Q}$. Then, using the functional version of the PIRLS algorithm, and thanks to Propositions 4.1 and 4.2, we obtain the following expressions for the maximizers $\hat{\boldsymbol{\beta}}$ and $\hat{f}$ of the penalized log-likelihood (2.2):

$$\hat{\boldsymbol{\beta}} = (\mathbf{X}^t \mathbf{W} \mathbf{X})^{-1} \mathbf{X}^t \mathbf{W} (\mathbf{I} - \mathbf{S}) \mathbf{z},$$

$\hat{f}$ is identified by the vector

$$\hat{\mathbf{f}} = \left(\boldsymbol{\Psi}^t \ \mathbf{Q} \ \boldsymbol{\Psi} + \lambda \boldsymbol{P} \right)^{-1} \boldsymbol{\Psi}^t \mathbf{Q} \mathbf{z}, \qquad (4.6)$$

and the vector of evaluations of $\hat{f}$ at the n data locations is given by

$$\hat{\mathbf{f}}_n = \boldsymbol{\Psi} \hat{\mathbf{f}} = \boldsymbol{\Psi} \left(\boldsymbol{\Psi}^t \ \mathbf{Q} \ \boldsymbol{\Psi} + \lambda \boldsymbol{P} \right)^{-1} \boldsymbol{\Psi}^t \mathbf{Q} \mathbf{z} = \mathbf{S} \mathbf{z},$$

where the vector of pseudo-data $\mathbf{z}$, and the matrices $\mathbf{W}, \mathbf{Q}$ and $\mathbf{S}$ are those obtained at the convergence of the PIRLS algorithm.

The positive definite matrix $\boldsymbol{P}$ represents the discretization of the penalty term in (2.2) and (4.1). Notice that, thanks to the variational formulation (4.3) of the estimation problem, this penalty matrix does not involve the computation of second-order derivatives. Azzimonti et al. [2015] shows that, in the finite element space used to discretize the problem, $\boldsymbol{P}$ is in fact equivalent to the penalty matrix that would be obtained as direct discretization of the penalty term in (2.2) and (4.1), and involving the computation of second-order derivatives.

We can define the hat (or influence) matrix $\mathbf{M}$ for the generalized additive model [see Hastie and Tibshirani, 1990, p. 156] as the matrix satisfying:

$$\hat{\boldsymbol{\theta}} = \mathbf{M} \mathbf{z},$$

where $\hat{\boldsymbol{\theta}}$ and $\mathbf{z}$ are respectively the canonical parameter and the pseudo-data at the convergence of the PIRLS algorithm. In this case, the hat matrix is given by:

$$\mathbf{M} = (\mathbf{H} + \mathbf{Q} \mathbf{S}).$$

The trace of the influence matrix can be used as measure of the equivalent degrees of freedom of the model [Buja et al., 1989]. Finally, the fitted mean is given by:

$$\hat{\boldsymbol{\mu}} = g^{-1}(\hat{\boldsymbol{\theta}}) = g^{-1}(\mathbf{Mz}).$$

4.5 Estimation of the scale parameter and selection of the smoothing parameter

Any distribution of the exponential family is described by two parameters, the mean μ and the scale parameter ϕ. The estimation of the mean does not require the estimation of the scale parameter but only of the canonical parameter. To estimate the scale parameter, we must estimate the mean for all the observations. A classical estimator of the scale parameter is [see, e.g., Wood, 2006]:

$$\hat{\phi} = \frac{\|\mathbf{V}^{-1/2}(\mathbf{y} - \hat{\boldsymbol{\mu}})\|^2}{n - \text{tr}(\mathbf{M})}, \tag{4.7}$$

where $\hat{\boldsymbol{\mu}}$ is the estimated mean at the convergence, $\mathbf{V}$ is the $n \times n$ diagonal matrix with entries $V(\hat{\mu}_1), \ldots, V(\hat{\mu}_n)$ and $\mathbf{M}$ is the hat matrix. We may choose the smoothing parameter λ by minimizing the Generalized Cross Validation (GCV) criterion [Craven and Wahba, 1978]:

$$\text{GCV}(\lambda) = \frac{n\|\mathbf{y} - \boldsymbol{\mu}(\hat{\boldsymbol{\beta}}, \hat{\mathbf{f}})(\lambda)\|^2}{[n - \gamma \, \text{tr}[\mathbf{M}(\lambda)]]^2}, \tag{4.8}$$

where $\boldsymbol{\mu}(\hat{\boldsymbol{\beta}}, \hat{\mathbf{f}})(\lambda)$ is the fitted mean at the convergence of the algorithm, for a fixed λ, and γ is a constant factor usually set equal to 1. In some cases, the GCV optimum leads to overfitting, so it can be useful to give more weight to the equivalent degrees of freedom of the model setting $\gamma \geq 1$.

As discussed extensively in Wood [2006], two alternative schemes can be adopted for the selection of the smoothing parameter when using a PIRLS algorithm. The parameter estimation can be done as a step of the PIRLS algorithm, leading to an update of the value of λ at each iteration of the algorithm; alternatively, the update of the smoothing parameter can be done at the convergence of the algorithm. These two different approaches are refereed to as *performance iteration* and *outer iteration* respectively. In this work we shall use an outer iteration scheme.

5 Model version for areal data

The proposed model can also be specified for the case of areal observations. Specifically, let $D_1, \ldots, D_n$ be disjoints subregions of the domain Ω. Over each subdomain D_i, we observe the realization y_i of a real variable of interest Y_i and a vector of covariate information $\mathbf{x}_i \in \mathbb{R}^q$. We assume $Y_1, \ldots, Y_n$ are

independent, with Y_i having a distribution within the exponential family, with mean μ_i and common scale paramenter ϕ. We now model μ_i by

$$g(\mu_i) = \mathbf{x}_i^t \boldsymbol{\beta} + \int_{D_i} f,$$

where the integral of the spatial field f over the subdomain D_i replace the pointwise evaluation of the field considered in model (2.1). We estimate $\boldsymbol{\beta} \in \mathbb{R}^q$ and the spatial field $f \in \mathcal{F}$ by maximizing a penalized log-likelihood functional in (2.2). If we redefine $\mathbf{f}_n$ as $\mathbf{f}_n = (\int_{D_1} f, \ldots, \int_{D_n} f)^t$, i.e., as being the vector of integrals of the spatial field over the subdomains, and we redefine the $n \times K$ matrix $\boldsymbol{\Psi}$ in (4.4) as the matrix with entry (i, j) given by $\int_{D_i} \psi_j$, then the derivation of the functional PIRLS algorithm, the implementation of the model and its properties follows as described in the previous sections for the geostatistical data case.

Appendix D presents in fact a more general formulation of the model proposed in this work, that comprehends as special cases the model version for geostatistical data and the one for areal data. The results detailed in the previous sections and in Appendices A, B and C, for the case of geostatistical data, carry over to this more general model, and thus also to the areal data case.

6 Simulation studies

6.1 Geostatistical data

In order to illustrate the good performances of the proposed model, we show some simulations on a horseshoe domain [Ramsay, 2002, Wood et al., 2008] and using the spatial test field shown in the top left panel of Figure 3, that is detailed in Appendix E. We consider an outcome with a gamma distribution; in this case, we need to estimate both the canonical and the scale parameter. We generate $n = 200$ data locations uniformly on the horseshoe. We then consider these locations as fixed. For each sampled data location $\mathbf{p}_i$, we generate two independent covariates x_{1i} and x_{2i} having a translated beta distribution; specifically we set $x_{1i} = 1 + u_{1i}$ and $x_{2i} = 1 + u_{2i}$, where $u_{1i} \overset{iid}{\sim} \text{Beta}(1.5, 2)$ and $u_{2i} \overset{iid}{\sim} \text{Beta}(3, 2)$. We set $\beta_1 = -\frac{2}{5}$ and $\beta_2 = \frac{3}{10}$. For each sampled data location $\mathbf{p}_i$, we then generate independent gamma random variables, with mean $\mu_i = -(\mathbf{x}_i^t \boldsymbol{\beta} + f(\mathbf{p}_i))^{-1}$ and common scale parameter ϕ. We repeat this simulation $M = 100$ times.

The top right panel of Figure 3 shows the sampled data in the first simulation repetition, with the size of the point marker proportional to data values. The bottom center and right panels of the same Figure displays the scatter plots of the response versus the two covariates; from these plots is not apparent that the two covariates are significant in explaining the response.
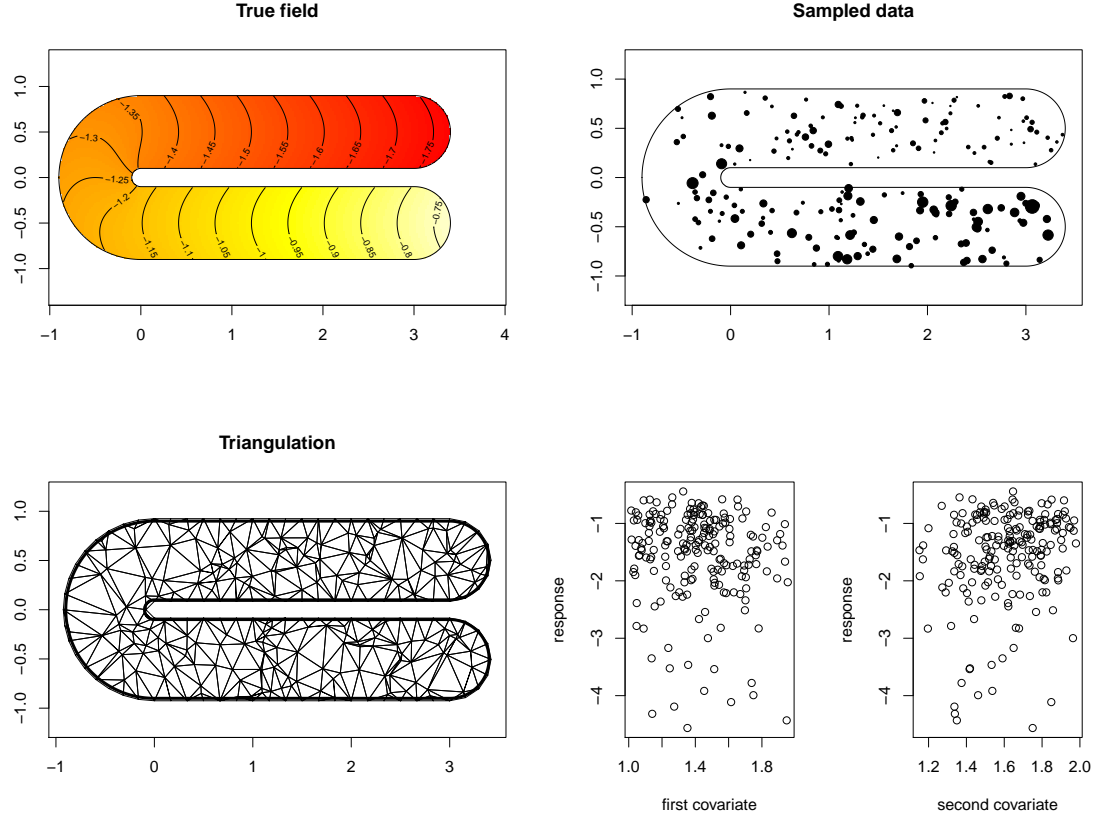
13

Figure 3: Simulation with geostatistical data. Top left: the true field f to be estimated. Top right: the data sampled in the first simulation repetition; the marker size is proportional to data values; the data locations are considered as fixed. Bottom left: the triangulation used to obtain the GSR-PDE estimate; this is a contrained Delaunay triangulation of the locations of the data shown in the top right panel. Bottom center and bottom right: scatter plots of the response versus the two covariates, for the first simulation repetition.
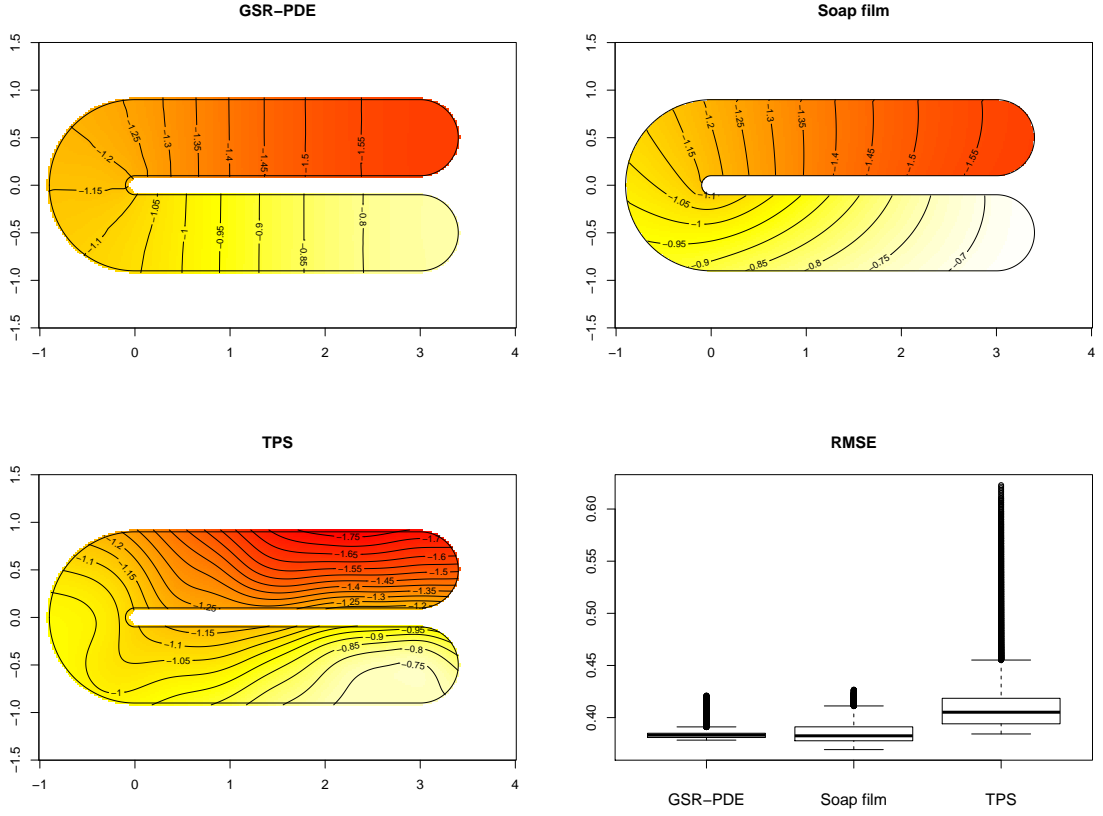
Figure 4: Simulation with geostatistical data. Estimates of the spatial field obtained in the first simulation repetition by GSR-PDE (top left), Soap film (top right) and TPS (bottom left). On the bottom right, the boxplot of the spatial distributions of the RMSE of the three spatial field estimators over the $M = 100$ simulation repetitions, computed on a fine grid of points over the horseshoe domain.

15

We compare our method to soap film smoothing [Wood et al., 2008] and to the thin-plate splines [Duchon, 1977, Wahba, 1990], implemented using the **R** package `mgcv` [Wood, 2013]. Soap film smoothing uses 72 degrees of freedom, as in the implementation given in the reference manual of the `mgcv` package (see function `Predict.matrix.soap.film`). Thin-plate splines (TPS) uses the default settings with 40 degrees of freedom. For the proposed GSR-PDE method, we use linear finite elements with a triangular mesh that is a constrained Delaunay triangulation of the n data locations; see Figure 3, bottom left panel. To ensure that the comparison is fair, at each simulation repetition we select the smoothing parameter for each of the considered methods optimizing the GCV criterion in an outer iteration scheme.

The root mean squared error (RMSE), over the $M = 100$ simulation repetitions, of the estimators of $\boldsymbol{\beta}$ are comparable accross the three considered methods (the RMSE of $\hat{\beta}_1$ are: 0.151 for GRS-PDE, 0.150 for Soap and 0.159 for TPS; the RMSE of $\hat{\beta}_2$ are: 0.178 for GRS-PDE, 0.174 for Soap and 0.178 for TPS). The bottom right panel of Figure 4 shows the boxplots of the spatial distribution of the RMSE, over the $M = 100$ simulation repetitions, of the estimators of the spatial field $\hat{f}$; specifically, we consider a fine grid of points $\mathbf{p}$, of step 0.02 in the x-direction and 0.01 in the y-direction, and for each of these points $\mathbf{p}$ we compute

$$\mathrm{RMSE}(\mathbf{p}) = \sqrt{\frac{1}{M} \sum_{j=1}^{M} \left(\hat{f}(\mathbf{p}) - f(\mathbf{p}) \right)^2}.$$

These boxplots show that the proposed GRS-PDE method and Soap film smoothing provide significantly better estimates than thin-plate splines. The reason of this comparative advantage is highlighted by the spatial field estimates returned by the three methods in the first simulation replicate, shown in the first three panels of Figure 4. The thin-plate spline technique is blind to the shape of the domain and smooths across the internal boundaries: the higher values of the field in one side of the horseshoe domain are smoothed with the lower values of the field in the other side of the domain, returning an highly biased estimate. The proposed GRS-PDE method and soap film smoothing do not suffer this problem, accurately complying with the domain geometry. The proposed GRS-PDE method is the best technique in terms of RMSE of the spatial field estimator.

6.2   Areal data

We now present a simulation with areal data. We consider the test function of the horseshoe domain displayed in the left panel of Figure 5 and detailed in Appendix E. The bottom left panel of the same figure shows in red the borders of the $n = 142$ sub-domains D_i considered. Indipendently over each subdomain D_i, we generate a covariate x_i having beta distribution:
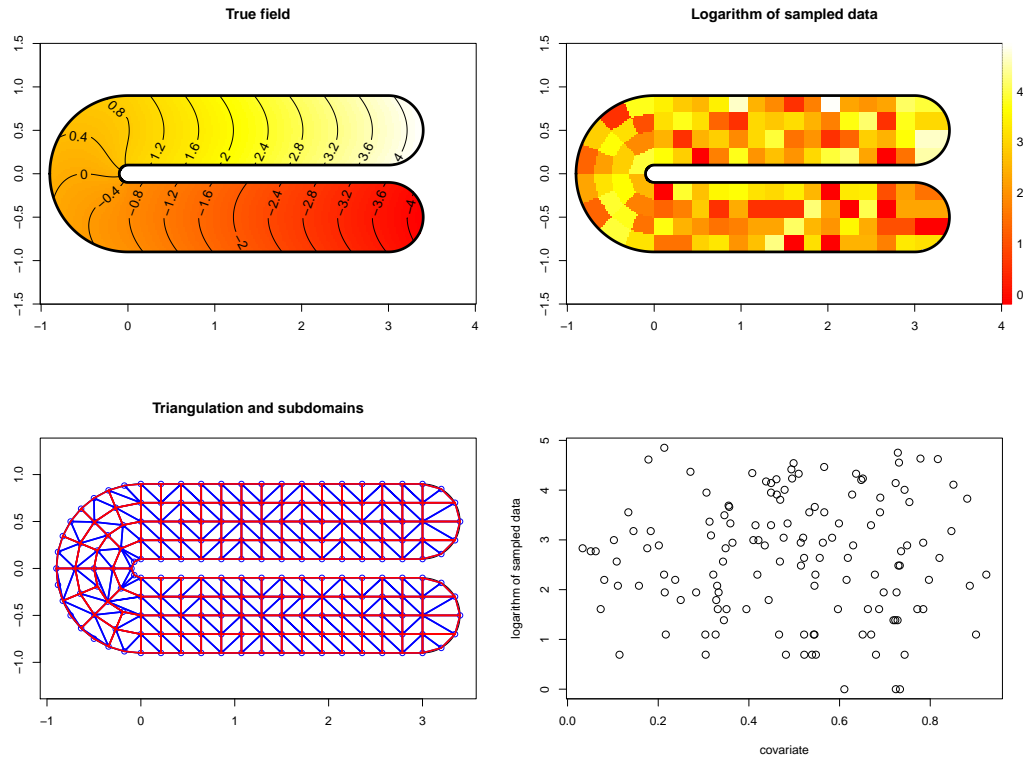
Figure 5: Simulation with areal data. Top left: the true field to be estimated. Top right: the logarithm of sampled data. Bottom left: the triangulation used to obtain the GSR-PDE estimate, with the borders of the subdomains highlighted in red. Bottom right: scatter plots of the response versus the covariate.

17

$x_i \overset{iid}{\sim} \text{Beta}(2,2)$. We set $\beta = 5$. Over each subdomain D_i, we the generate independent Poisson random variables with mean μ_i, where $\log(\mu_i) = \mathbf{x}_i^t \boldsymbol{\beta} + \int_{D_i} f$. Notice that in this case the scale parameter is 1 and does not need to be estimated. The simulation is repeated $M = 100$ times.

The top right panel of Figure 5 shows the sampled data in the first simulation repetition (in logarithmic scale); the bottom right panel of the same Figure displays a scatter plot of the response (in logarithmic scale) versus the covariate.
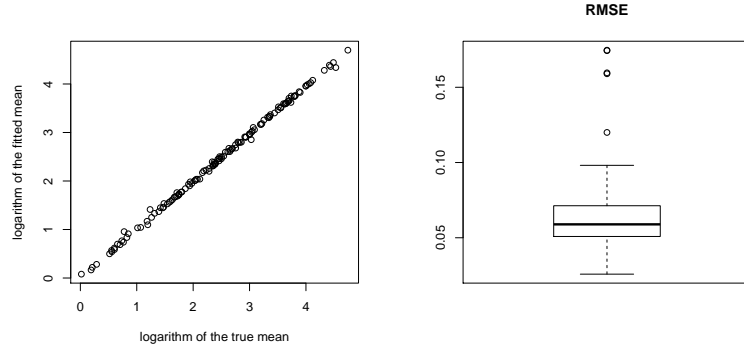

Figure 6: Simulation with areal data. Left: scatter plot of the the estimated mean vs the true mean over each subdomain, for the first simulation repetition. Right: boxplot of the spatial distribution of the RMSE, over the $M = 100$ simulation repetitions, of the non-parametric part of the model, computed over each subdomain as detailed in eq. (6.1).
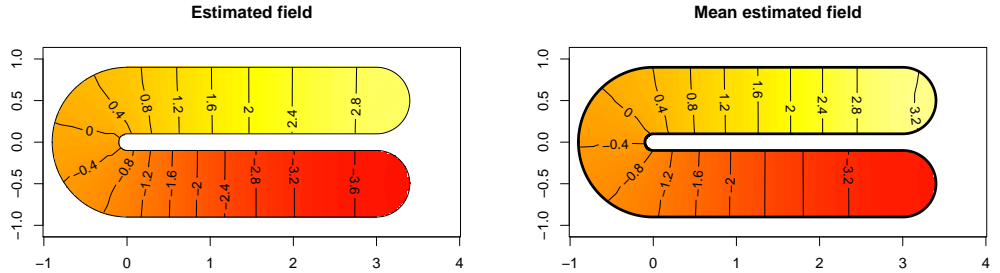

Figure 7: Simulation with areal data: Left: estimated spatial field in the first simulation repetition. Right: mean of the estimated spatial fields over the $M = 100$ simulation repetitions.

The sample mean of the estimated $\hat{\beta}$ coefficient over the $M = 100$ simulation repetitions is 5.021 (true value: 5) with a standard deviation of 0.073 and a RMSE of 0.076. The left panel of Figure 6 compares the log estimated

mean over each subdomain in the first simulation repetition, and the true one, showing the very good performances of the method. The right panel of the same figure displays the boxplot of the spatial distribution of the RMSE, over the $M = 100$ simulation repetitions, of the non-parametric part of the model, computed over each sub-domain as

$$\text{RMSE}(D_i) = \sqrt{\frac{1}{M} \sum_{j=1}^{M} \left(\int_{D_i} \hat{f} - \int_{D_i} f \right)^2} \qquad (6.1)$$

for $i = 1, \ldots, n = 142$. Finally, Figure 7 shows the estimated field $\hat{f}$ in the first simulation repetition and the sample mean of the estimated spatial field over the 100 simulation repetitions. These highlight that the method is able to recover quite well the pointwise values of the field, even though using only areal observations. The estimates of β and of f appear to have a negligible bias and a small variance.

7   Application: Crimes in Portland

The city of Portland, Oregon (USA) has made publicly available a data set about all crimes committed in the city in 2012[1]. We would like to study the criminality over this city, taking into account auxiliary census information[2]. The census information (year 2010) is aggregated at the level of the neighborhoods. Here in particular we consider as covariate the total population of each neighborhood. The map of Portland in the left panel of Figure 1 highlights in blue the borders of these neighborhoods, together with the locations of crimes. For computational simplicity, the triangulation of the city territory shown in the right panel of the same figure has been constructed in a way to comply with the borders of the neighborhoods. Since the covariate is only available at the level of neighborhoods, we decided to aggregate also the crimes, thus considering as response variable the total crime count over each neighborhood. We model these data as an inhomogeneous Poisson process. Specifically, the total crime counts $Y_1, \ldots, Y_n$ over the $n = 98$ neighborhoods are modeled as independent Poisson random variables with mean μ_i, where

$$\log(\mu_i) = \log(\texttt{pop}_i)\beta + \int_{D_i} f \ dx,$$

and $\texttt{pop}_i$ denotes the total population over the i-th neighborhood.

We select the smoothing parameter via the GCV criterion. We get $\hat{\beta} = 0.381$, confirming that the population density contributes positively to the crimes count in a given neighborhood. Figure 8 compares, in a logarithm

---

[1]Portland crime data: http://www.civicapps.org/datasets
[2]Census Bureau Data: http://www.portlandoregon.gov/oni/28387

scale, the observed and estimated crime densities over each neighborhood, where the density is computed as the total crime count over the neighborhood divided by the area of the neighborhood. These are also compared in the scatter plot in the left panel of Figure 9, highlighting the goodness of fit of the model. Finally, the right panel of Figure 9 shows the estimated spatial field. When the estimated field is close to zero, the crimes count is well described by the parametric part of the model, namely as a rate of the number of residents. The highest levels of the estimated spatial field are located dowtown; this is likely due to the high number of people who come to the city center for work or leisure during the day and in the evening. The estimate complies with the complex shape of the domain.
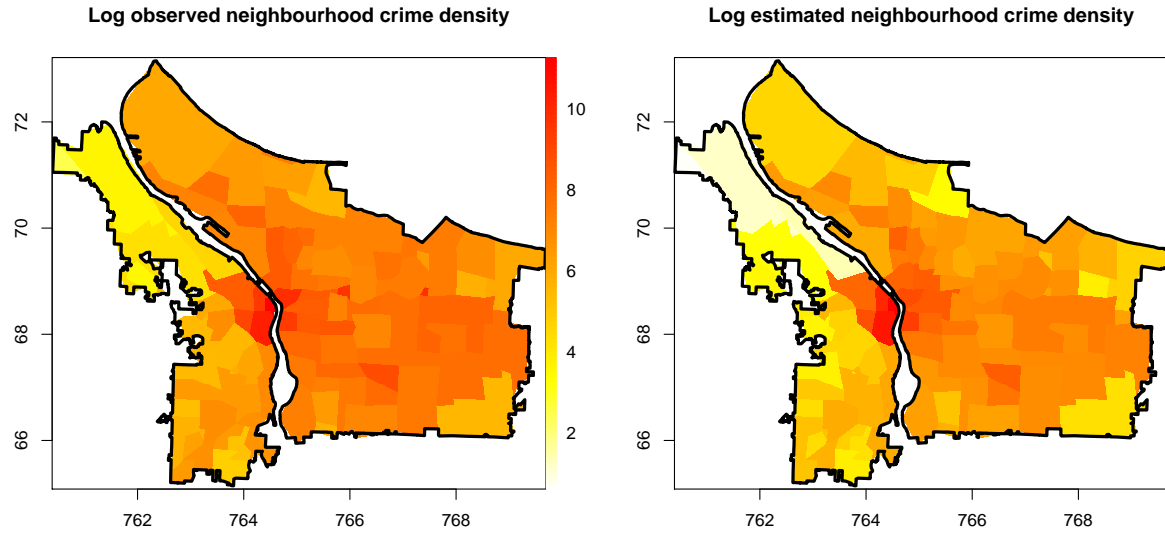

Figure 8: Log of observed crime density over each neighborhood (left) and corresponding log of estimated crime density (right).
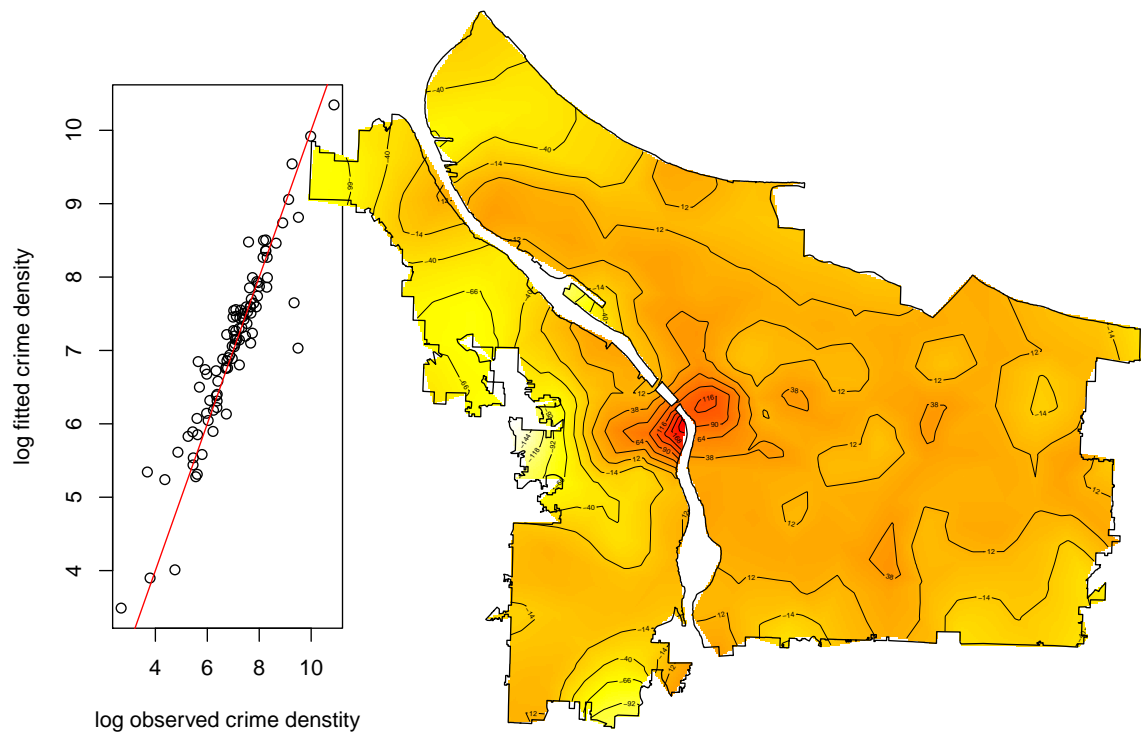
Figure 9: Left: fitted crime density per neighborhoods vs observed one, in a logarithmic scale. Right: estimated spatial field f over the city of Portland.

8 Discussions

The method proposed can be extended in various directions. First of all, owing to the functional version of the PIRLS algorithm, our methodology can be extended to more complex roughness penalties. This is particularly interesting when a priori knowledge is available on the problem under study, that can be formalized in terms of a partial differential equation modeling the phenomenon behavior. Azzimonti et al. [2015] shows for instance that in some applications using a penalty based on a priori knowledge about the problem can dramatically improve the accuracy of the estimation. By using more complex roughness penalties we can also account for spatial anisotropy and non-stationarity. See also Appendix A. Moreover, as mentioned in Section 4, it is possible to use different kinds of boundary conditions, allowing for a very flexible modelling of the behavior of the spatial field at the boundary of the domain of interest.

Furthermore, following the approach developed in Ettinger et al. [2016], the proposed method could be extended to deal with data distributed over curved domains, specifically over surface domains. This would permit to tackle important applications in the geosciences, dealing for instance with Poisson counts and other type of variables of interest observed over the globe or over regions with complex orography. Other fascinating fields of applications of this modeling extension would be in the neurosciences and other life sciences, studying for instance signals associated to neuronal activity over the cortical surface, the highly convoluted thin sheet of neural tissue that constitutes the outermost part of the brain.

Other numerical techniques and associated basis could also be used to solve the estimation problem, instead of the finite element method here considered. For instance, B-Splines and NURBS [Piegl and Tiller, 1997] are extensively used in computer-aided design (CAD), manufacturing, and engineering, to represent the 3D surface of the designed item. Wilhelm et al. [2016] offers a first example of a spatial data analysis model exploiting these basis, thus avoiding the domain approximation implied by finite elements. Extending this approach to the generalized linear setting here considered would further broaden the applicability of the proposed methodology to many engineering fields, including the automotive, the aircraft and the space sectors.

Aknowledgements

References

L. Azzimonti, F. Nobile, L. M. Sangalli, and P. Secchi. Mixed finite elements for spatial regression with PDE penalization. *SIAM/ASA Journal on Uncertainty Quantification*, 2(1):305–335, 2014.

L. Azzimonti, L. M. Sangalli, P. Secchi, M. Domanin, and F. Nobile. Blood flow velocity field estimation via spatial regression with PDE penalization. *Journal of the American Statistical Association*, 110(511):1057–1071, 2015.

W. Bernasco and H. Elffers. Statistical analysis of spatial crime data. In A.R. Piquero and D. Weisburd (eds.), editors, *Handbook of Quantitative Criminology*, pages 699–724. Springer New York, 2010.

A. Buja, T. J. Hastie, and R. J. Tibshirani. Linear smoothers and additive models. *The Annals of Statistics*, 17(2):453–510, 1989.

S. Chainey and J. Ratcliffe. *GIS and crime mapping*. John Wiley & Sons, 2005.

P. Craven and G. Wahba. Smoothing noisy data with spline functions. *Numerische Mathematik*, 31(4):377–403, 1978.

P. Diggle and P. J. Ribeiro. *Model-based Geostatistics*. Springer Series in Statistics. Springer, 2007.

J. Duchon. Splines minimizing rotation-invariant semi-norms in sobolev spaces. In Walter Schempp and Karl Zeller, editors, *Constructive Theory of Functions of Several Variables*, volume 571 of *Lecture Notes in Mathematics*. Springer Berlin Heidelberg, 1977.

B. Ettinger, S. Perotto, and L. M. Sangalli. Spatial regression models over two-dimensional manifolds. *Biometrika*, 103(1):71–88, 2016.

T. J. Hastie and R. J. Tibshirani. *Generalized Additive Models*. Monographs on Statistics and Applied Probability Series. Chapman & Hall, CRC Press, 1990.

F. Lindgren, H. Rue, and J. Lindstrom. An explicit link between gaussian fields and gaussian markov random fields: the stochastic partial differential equation approach (with discussion). *Journal of the Royal Statistical Society: Series B (Statistical Methodology)*, 73(4):423–498, 2011.

G. Marra and S. N. Wood. Coverage properties of confidence intervals for generalized additive models components. *Scandinavian Journal of Statistics*, 939, 2012.

P. McCullagh and J. A. Nelder. *Generalized Linear Models*. Chapman & Hall, Boca-Raton, 1989.

F. O'Sullivan, B. S. Yandell, and Jr. Raynor, W. J. Automatic smoothing of regression functions in generalized linear models. *Journal of the American Statistical Association*, 81(393):96–103, 1986.

L. Piegl and W. Tiller. *The NURBS Book*. Springer-Verlag, New York, 1997.

A. Quarteroni. *Numerical Models for Differential Problems*. MS&A (Series). Springer-Verlag Milan, 2014.

J. O. Ramsay. Differential equation models for statistical functions. *Canadian Journal of Statistics*, 28(2):225–240, 2000.

T. O. Ramsay. Spline smoothing over difficult regions. *Journal of the Royal Statistical Society: Series B (Statistical Methodology)*, 64(2):307–319, 2002.

J. Ratcliffe. Crime mapping: spatial and temporal challenges. In A.R. Piquero and D. Weisburd (eds.), editors, *Handbook of Quantitative Criminology*, pages 5–24. Springer New York, 2010.

L. M. Sangalli, J. O. Ramsay, and T. O. Ramsay. Spatial spline regression models. *Journal of the Royal Statistical Society: Series B (Statistical Methodology)*, 75(4):681–703, 2013.

G. Wahba. *Spline Models for Observational Data*. Society for Industrial and Applied Mathematics, Philadelphia, 1990.

M. Wilhelm, L. Dedè, L. M. Sangalli, and P. Wilhelm. IGS: an IsoGeometric approach for Smoothing on surfaces. *Computer Methods in Applied Mechanics and Engineering*, 302:70–89, 2016.

S. N. Wood. *Generalized additive models: an introduction with application in R*. Springer Series in statistics. Springer, 2006.

S. N. Wood, M. V. Bravington, and S. L. Hedley. Soap film smoothing. *Journal of the Royal Statistical Society: Series B (Statistical Methodology)*, 70(5):931–955, 2008.

S.N. Wood. *mgcv: Mixed GAM Computation Vehicle with GCV/AIC/REML smoothness estimation*, 2013. R package version 1.7-27.

A   On the spatial variation structure of the estimator

Let us focus on the special case of the proposed model, where the outcomes y_i are normally distributed with mean $\mu_i = \theta_i = x_i^t \boldsymbol{\beta} + f(\mathbf{p}_i)$ and constant variance σ^2. In this case, the maximization of the penalized log-likelihood function is equivalent to the minimization of the penalized least-square functional considered in Sangalli et al. [2013] and the quadratic form of the functional allows to characterize analytically the solution to the estimation problem, so that there is no need to resort to the functional version of the PIRLS algorithm. Specifically, the estimator $\hat{f}$ of the spatial field is identified by the vector

$$\hat{\mathbf{f}} = \left(\boldsymbol{\Psi}^t \mathbf{Q} \boldsymbol{\Psi} + \lambda \boldsymbol{P} \right)^{-1} \boldsymbol{\Psi}^t \mathbf{y}, \tag{A.1}$$

where the vector of observed data values $\mathbf{y}$ has replaced the vector of speudo-data $\mathbf{z}$ that is found in equation (4.6); the matrix $\mathbf{Q} = \mathbf{I} - \mathbf{H}$ represents the contribution of the parametric part of the model, where now $\mathbf{H} = \mathbf{X}(\mathbf{X}^t\mathbf{X})^{-1}\mathbf{X}^t$. In this case, the estimator of the spatial field is linear in the observed data values, and has a typical penalized regression form, $\boldsymbol{P}$ being the discretization of the regularizing term. From (A.1), it follows that the estimate of the field f at any generic location $\mathbf{p} \in \Omega$ is given by

$$\hat{f}(\mathbf{p}) = \boldsymbol{\psi}(\mathbf{p})^t (\boldsymbol{\Psi}^t \boldsymbol{\Psi} + \boldsymbol{P})^{-1} \boldsymbol{\Psi}^t \mathbf{y}.$$

Its mean and variance are given by

$$\begin{aligned}
E[\hat{f}(\mathbf{p})] &= \boldsymbol{\psi}(\mathbf{p})^t (\boldsymbol{\Psi}^t \boldsymbol{\Psi} + \boldsymbol{P})^{-1} \boldsymbol{\Psi}^t \hat{\mathbf{f}}_n \\
Var[\hat{f}(\mathbf{p})] &= \sigma^2 \boldsymbol{\psi}(\mathbf{p})^t (\boldsymbol{\Psi}^t \boldsymbol{\Psi} + \boldsymbol{P})^{-1} \boldsymbol{\Psi}^t \boldsymbol{\Psi} (\boldsymbol{\Psi}^t \boldsymbol{\Psi} + \boldsymbol{P})^{-1} \boldsymbol{\psi}(\mathbf{p})
\end{aligned}$$

and the covariance at any two locations $\mathbf{p}_1, \mathbf{p}_2 \in \Omega$ is given by

$$Cov[\hat{f}(\mathbf{p}_1,), \hat{f}(\mathbf{p}_2)] = \sigma^2 \boldsymbol{\psi}(\mathbf{p}_1)^t (\boldsymbol{\Psi}^t \boldsymbol{\Psi} + \boldsymbol{P})^{-1} \boldsymbol{\Psi}^t \boldsymbol{\Psi} (\boldsymbol{\Psi}^t \boldsymbol{\Psi} + \boldsymbol{P})^{-1} \boldsymbol{\psi}(\mathbf{p}_2).$$

The above expressions highlight that both the first order structure and the second order structure of the field estimator are determined by the penalization term. The regularizing term considered in this work induces an isotropic and stationary space variation. Different regularizations would imply different mean and covariance structures for the field estimator. For instance, Azzimonti et al. [2015] consider a regularized spatial regression model and show that by changing the regularizing terms and considering more complex differential operators it is possible to include in the model a priori information about the spatial variation of the phenomenon, and model also space

anisotropies and non-stationarities. The estimator $\hat{\boldsymbol{\beta}}$ is also linear in the observed data values and it is straightforward to compute its distributional properties.

Outside of the Gaussian case, it is not possible to characterize analytically the solution of the estimation problem. Nevertheless, at each iteration of the functional PIRLS algorithm, the field estimator has the same form and properties reported above, with respect to the pseudo-data $\mathbf{z}$. Hence, also in this more general case, the regularizing term implies the first and second order structure of the estimator. Quantification of uncertainty is in this case possible using the techniques developed for generalized additive models; see, e.g., Hastie and Tibshirani [1990] and Wood [2006]. Bayesian approaches are also available in this context; see, e.g., Marra and Wood [2012].

B Proof of the functional justification of PIRLS algorithm

Using the notation given in Section 3, we want to maximize the penalized log-likelihood function $\mathcal{L}_p(\boldsymbol{\beta}, f)$ of any exponential family distribution, which is given by:

$$\mathcal{L}_p(\boldsymbol{\beta}, f) = \mathcal{L}(\boldsymbol{\beta}, f) - \frac{\lambda}{2} m(f, f) = \sum_{i=1}^{n} y_i \theta_i(\boldsymbol{\beta}, f) - b(\theta_i(\boldsymbol{\beta}, f)) - \frac{\lambda}{2} m(f, f),$$

where $\mathcal{L}$ is the likelihood of an exponential family distribution, $b(\cdot)$ is a function depending on the distribution considered and $\theta_i(\boldsymbol{\beta}, f) = g(\mathbf{x}_i^t \boldsymbol{\beta} + f(\mathbf{p}_i))$ is the canonical parameter. The maximizers $(\hat{\boldsymbol{\beta}}, \hat{f})$ of the functional (2.2) must satisfy the following system of first order equations:

$$\begin{cases} \dfrac{\partial \mathcal{L}(\hat{\boldsymbol{\beta}}, \hat{f})}{\partial \beta_k} &= 0, \quad \forall k = 1, \ldots, q, \\[2ex] \lim_{t \to 0} \dfrac{1}{t} \left[\mathcal{L}(\hat{\boldsymbol{\beta}}, \hat{f} + tu) - \mathcal{L}(\hat{\boldsymbol{\beta}}, \hat{f}) \right] - \lambda\, m(u, \hat{f}) &= 0 \quad \forall u \in \mathcal{F}. \end{cases}$$
(B.1)

This system involves the derivatives with respect to both parameters $\boldsymbol{\beta}$ and f. The derivative with respect to f is a Gâteaux derivative in the direction of u, where $u \in \mathcal{F}$. In particular, $m(u, \hat{f})$ is the derivative of the term $m(\hat{f}, \hat{f})$. We then have to compute the terms involving $\mathcal{L}$ only. We first compute:

$$\mathcal{L}(\boldsymbol{\beta}, f + tu) - \mathcal{L}(\boldsymbol{\beta}, f) =$$
$$= \sum_{i=1}^{n} \frac{1}{\phi} \left[(y_i \theta_i(\boldsymbol{\beta}, f + tu) - b(\theta_i(\boldsymbol{\beta}, f + tu)) - y_i \theta_i(\boldsymbol{\beta}, f) + b(\theta_i(\boldsymbol{\beta}, f))) \right]$$
$$= \sum_{i=1}^{n} \frac{1}{\phi} \left(y_i \theta_i(\boldsymbol{\beta}, f + tu) - y_i \theta_i(\boldsymbol{\beta}, f) - (b(\theta_i(\boldsymbol{\beta}, f + tu)) - b(\theta_i(\boldsymbol{\beta}, f))) \right).$$

Dividing this expression by t and taking the limit as t tends to 0 gives the Gâteaux derivative of $\mathcal{L}(\boldsymbol{\beta}, f)$ in the direction of u, denoted by $\frac{\partial \mathcal{L}(\boldsymbol{\beta}, u)}{\partial f}$. We have then:

$$
\begin{aligned}
\frac{\partial \mathcal{L}(\boldsymbol{\beta}, u)}{\partial f} &= \lim_{t \to 0} \frac{1}{t} \left[\mathcal{L}(\boldsymbol{\beta}, f + tu) - \mathcal{L}(\boldsymbol{\beta}, f) \right] \\
&= \lim_{t \to 0} \frac{1}{t} \left(\sum_{i=1}^{n} \frac{1}{\phi} \left[y_i \theta_i(\boldsymbol{\beta}, f + tu) - y_i \theta_i(\boldsymbol{\beta}, f) - (b(\theta_i(\boldsymbol{\beta}, f + tu)) - b(\theta_i(\boldsymbol{\beta}, f))) \right] \right) \\
&= \sum_{i=1}^{n} \frac{1}{\phi} \left[y_i \frac{\partial \theta_i(\boldsymbol{\beta}, u)}{\partial f} - \frac{\partial b}{\partial \theta}(\theta_i(\boldsymbol{\beta}, f)) \frac{\partial \theta_i(\boldsymbol{\beta}, u)}{\partial f} \right].
\end{aligned}
$$

We then need to compute $\frac{\partial \theta_i(\boldsymbol{\beta}, u)}{\partial f}$. We recall that, for a distribution within the exponential family, $\mathbb{E}\left[Y_i\right] = \mu_i = \frac{\partial b(\theta_i)}{\partial \theta}$ and $\mathrm{var}(Y_i) = \frac{\partial^2 b(\theta)}{\partial \theta^2} \phi$. We thus have:

$$
\frac{\partial \mu}{\partial \theta} = \frac{\partial^2 b}{\partial \theta^2} \Rightarrow \frac{\partial \theta}{\partial \mu} = \frac{1}{\frac{\partial^2 b}{\partial \theta^2}}
$$

and hence:

$$
\frac{\partial \theta_i(\boldsymbol{\beta}, u)}{\partial f} = \frac{1}{\frac{\partial^2 b(\theta_i(\boldsymbol{\beta}, u))}{\partial \theta^2}} \frac{\partial \mu_i(\boldsymbol{\beta}, u)}{\partial f}.
$$

We can therefore conclude that:

$$
\frac{\partial \mathcal{L}(\boldsymbol{\beta}, u)}{\partial f} = 0 \Leftrightarrow \sum_{i=1}^{n} \frac{1}{\phi} \frac{(y_i - \frac{\partial b(\theta_i)}{\partial \theta})}{\frac{\partial^2 b(\theta_i)}{\partial \theta^2}} \frac{\partial \mu_i(\boldsymbol{\beta}, u)}{\partial f} = \sum_{i=1}^{n} \frac{(y_i - \frac{\partial b(\theta_i)}{\partial \theta})}{\mathrm{var}(Y_i)} \frac{\partial \mu_i(\boldsymbol{\beta}, u)}{\partial f} = 0.
$$

Since we have $\mathrm{var}(Y_i) = V(\mu_i)\phi = \frac{\partial^2 b(\theta)}{\partial \theta^2} \phi$ and $\frac{\partial b(\theta_i)}{\partial \theta} = \mu_i$, we finally obtain the following expression for the derivative of the likelihood with respect to the functional parameter:

$$
\frac{\partial \mathcal{L}(\boldsymbol{\beta}, u)}{\partial f} = 0 \Leftrightarrow \sum_{i=1}^{n} \frac{(y_i - \mu_i)}{V(\mu_i)} \frac{\partial \mu_i(\boldsymbol{\beta}, u)}{\partial f} = 0. \tag{B.2}
$$

We now need to compute the derivative of the likelihood with respect to β_j:

$$
\frac{\partial \mathcal{L}(\boldsymbol{\beta})}{\partial \beta_j} = \sum_{i=1}^{n} \frac{1}{\phi} \left(y_i \frac{\partial \theta_i}{\partial \beta_j} - \frac{\partial b(\theta_i)}{\partial \theta} \frac{\partial \theta_i}{\partial \beta_j} \right).
$$

Since

$$
\frac{\partial \theta_i}{\partial \beta_j} = \frac{\partial \theta_i}{\partial \mu_i} \frac{\partial \mu_i}{\partial \beta_j} = \frac{1}{\frac{\partial^2 b(\theta_i)}{\partial \theta^2}} \frac{\partial \mu_i}{\partial \beta_j},
$$

and using similar computations, we finally get:

$$
\frac{\partial \mathcal{L}(\boldsymbol{\beta})}{\partial \beta_j} = 0 \Leftrightarrow \sum_{i=1}^{n} \frac{(y_i - \mu_i)}{V(\mu_i)} \frac{\partial \mu_i}{\partial \beta_j} = 0. \tag{B.3}
$$

27

Putting (B.2) and (B.3) together implies that the solution to (B.1) is equivalent to finding $\boldsymbol{\mu} = \boldsymbol{\mu}(\boldsymbol{\beta}, f)$ that satisfies

$$
\begin{cases}
\displaystyle\sum_{i=1}^{n} \frac{(y_i - \mu_i)}{V(\mu_i)} \frac{\partial \mu_i}{\partial \beta_j} &=& 0, \quad \forall j = 1, \ldots, q, \\
\displaystyle\sum_{i=1}^{n} \frac{(y_i - \mu_i)}{V(\mu_i)} \frac{\partial \mu_i(\boldsymbol{\beta}, u)}{\partial f} + \lambda\, m(f, u) &=& 0 \quad \forall u \in \mathcal{F}.
\end{cases}
\tag{B.4}
$$

If we now assumed that $V(\mu_i)$ is constant, solving (B.4) would be equivalent to finding the minimizers of the following functional

$$
\mathcal{J}_\lambda(\boldsymbol{\beta}, f) = \|\mathbf{V}^{-1/2}\,(\mathbf{y} - \boldsymbol{\mu})\,\|^2 + \lambda\, m(f, f),
$$

where $\mathbf{V}$ is the $n \times n$ diagonal matrix with entries $V(\mu_1), \ldots, V(\mu_n)$. Since in reality $\mathbf{V}$ depends on $\boldsymbol{\mu}$, this suggests an iterative computation scheme.

Let $\boldsymbol{\mu}^{(k)}$ be an estimate of $\boldsymbol{\mu}(\boldsymbol{\beta}, f)$ after k iterations of such a scheme. At this point, we consider a first order approximation of $\boldsymbol{\mu}$ in the neighbourhood of the current value $\boldsymbol{\mu}^{(k)} = (\boldsymbol{\beta}^k, f^{(k)})$:

$$
\boldsymbol{\mu}(\boldsymbol{\beta}, \mathbf{f}) \approx \underbrace{g^{-1}(\mathbf{X}\boldsymbol{\beta}^{(k)} + \mathbf{f}_n^{(k)})}_{=\boldsymbol{\mu}^{(k)}} + \frac{\partial \boldsymbol{\mu}(\boldsymbol{\beta}, f)}{\partial \boldsymbol{\beta}}(\boldsymbol{\beta} - \boldsymbol{\beta}^{(k)}) + \frac{\partial \boldsymbol{\mu}(\boldsymbol{\beta}, f - f^{(k)})}{\partial f}.
$$

We then have to compute the partial derivatives of $\boldsymbol{\mu}$ with respect to both parameters $\boldsymbol{\beta}$ and f. Let us start with the derivative with respect to $\boldsymbol{\beta}$. We have: $g(\mu_i^{(k)}) = \mathbf{x}_i^t \boldsymbol{\beta}^{(k)} + f(\mathbf{p}_i)$. Taking the derivative with respect to β_j on both sides, we get:

$$
g'(\mu_i^{(k)}) \frac{\partial \mu_i^{(k)}}{\partial \beta_j} = \frac{\partial}{\partial \beta_j} g(\mu_i^{(k)}) = \frac{\partial}{\partial \beta_j} \left(\mathbf{x}_i^t \boldsymbol{\beta}^{(k)} + f(\mathbf{p}_i) \right) = x_{ij},
$$

where x_{ij} is the jth component of the vector $\mathbf{x}_i$, or equivalently the ijth component of the design matrix $\mathbf{X}$. Then:

$$
\frac{\partial \mu_i^{(k)}}{\partial \beta_j} = \frac{x_{ij}}{g'(\mu_i^{(k)})}
$$

that in matrix form is:

$$
\frac{\partial \boldsymbol{\mu}(\boldsymbol{\beta}, f)}{\partial \boldsymbol{\beta}} = (\mathbf{G}^{(k)})^{-1}\mathbf{X},
$$

where $\mathbf{G}^{(k)}$ is the $n \times n$ diagonal matrix with entries $g'(\mu_1^{(k)}), \ldots, g'(\mu_n^{(k)})$.

Let us now compute the derivative $\boldsymbol{\mu}(\boldsymbol{\beta}, f)$, in the direction f. We first recall that $\boldsymbol{\mu}(\boldsymbol{\beta}, f) = g^{-1}(\boldsymbol{\theta}(\beta, f)$ and $\boldsymbol{\theta} = (\mathbf{X}\beta + \mathbf{f}_n)$. For the ith component,

we then obtain:

$$\lim_{t \to 0} \frac{\mu_i(\boldsymbol{\beta}^{(k)}, f^{(k)} + t(f - f^{(k)})) - \mu_i(\boldsymbol{\beta}^{(k)}, f^{(k)})}{t}$$

$$= \lim_{t \to 0} \frac{g^{-1}(\theta_i(\boldsymbol{\beta}^{(k)}, f^{(k)} + t(f - f^{(k)}))) - g^{-1}(\theta_i(\boldsymbol{\beta}^{(k)}, f^{(k)}))}{\theta_i(\boldsymbol{\beta}^{(k)}, f^{(k)} + t(f - f^{(k)})) - \theta_i(\boldsymbol{\beta}^{(k)}, f^{(k)})}$$

$$\cdot \frac{\theta_i(\boldsymbol{\beta}^{(k)}, f^{(k)} + t(f - f^{(k)})) - \theta_i(\boldsymbol{\beta}^{(k)}, f^{(k)})}{t}$$

$$= (g^{-1})'(\theta_i(\boldsymbol{\beta}^{(k)}, f^{(k)})) \left(f(\mathbf{p}_i) - f^{(k)}(\mathbf{p}_i) \right) = \frac{1}{g'(\mu_i^{(k)})} \left(f(\mathbf{p}_i) - f^{(k)}(\mathbf{p}_i) \right).$$

Hence, we finally have the following first order approximation of $\mathcal{J}_\lambda(\boldsymbol{\beta}, f)$ in the neighbourhood of the current value $\boldsymbol{\mu}^{(k)} = (\boldsymbol{\beta}^{(k)}, f^{(k)})$:

$$\tilde{\mathcal{J}}_\lambda^{(k)}(\boldsymbol{\beta}, f) = \| \mathbf{V}^{-1/2} \left[\mathbf{y} - \left(\boldsymbol{\mu}^{(k)} + (\mathbf{G}^{(k)})^{-1} \mathbf{X}(\boldsymbol{\beta} - \boldsymbol{\beta}^{(k)}) + (\mathbf{G}^{(k)})^{-1}(\mathbf{f}_n - \mathbf{f}_n^{(k)}) \right) \right] \|^2 + \lambda \, m(f, f)$$

$$= \| \mathbf{V}^{-1/2}(\mathbf{G}^{(k)})^{-1} \left(\mathbf{G}^{(k)}(\mathbf{y} - \boldsymbol{\mu}^{(k)}) + \mathbf{X}\boldsymbol{\beta}^{(k)} + \mathbf{f}_n^{(k)} - \mathbf{X}\boldsymbol{\beta} - \mathbf{f}_n \right) \|^2 + \lambda \, m(f, f)$$

Setting $\mathbf{z}^{(k)} = \mathbf{G}^{(k)}(\mathbf{y} - \boldsymbol{\mu}^{(k)}) + \mathbf{X}\boldsymbol{\beta}^{(k)} + \mathbf{f}_n^{(k)}$, and denoting by $\mathbf{W}^{(k)}$ the $n \times n$ diagonal matrix with ith entry $V(\mu_i^{(k)})^{-1} g'(\mu_i^{(k)})^{-2}$, we can rewrite

$$\tilde{\mathcal{J}}_\lambda^{(k)}(\boldsymbol{\beta}, f) = \| (\mathbf{W}^{(k)})^{1/2}(\mathbf{z}^{(k)} - \mathbf{X}\boldsymbol{\beta} - \mathbf{f}_n) \|^2 + \lambda \, m(f, f).$$

Since $\mathbf{W}^{(k)}$ is positive definite, $\tilde{\mathcal{J}}_\lambda$ is a quadratic form whose minimum exists and is unique.

C   Proof of Proposition 4.1

Before giving the proof of Proposition 4.1, we recall the Lax-Milgram theorem [see, e.g., Quarteroni, 2014]:

Theorem C.1 (Lax-Milgram). *Let $\mathcal{F}$ be a Hilbert space, $G(\cdot, \cdot) : \mathcal{F} \times \mathcal{F} \to \mathbb{R}$ a continuous and coercive bilinear form and $F : \mathcal{F} \to \mathbb{R}$ a linear and continuous functional. Then, there exists a unique solution of the following problem:*

find $u \in \mathcal{F}$ such that $G(u, v) = F(v), \; \forall v \in \mathcal{F}$.

Moreover, if $G(\cdot, \cdot)$ is symmetric, then $u \in \mathcal{F}$ is the unique minimizer in $\mathcal{F}$ of the functional $B : \mathcal{F} \to \mathbb{R}$, defined as

$$B(u) = G(u, u) - 2F(u).$$

We also need the following result.

Lemma C.1. *The bilinear and symmetric form* $G : H^2_{\mathbf{n}_0}(\Omega) \times H^2_{\mathbf{n}_0}(\Omega)$ *defined as*

$$G(v, u) = \mathbf{u}_n^t \mathbf{Q} \ \mathbf{v}_n + \lambda \int_\Omega (\Delta u)(\Delta v),$$

is continuous and coercive.

Proof. We recall the definition of the norm $\| \cdot \|_{H^2}$ and of the semi-norm $|\cdot|_{H^2}$:

$$\|u\|_{H^2} = \sum_{|\alpha| \leq 2} \|\partial^\alpha u\|_{L^2}, \quad |u|_{H^2} = \|\Delta u\|_{L^2}, \quad \forall u \in H^2.$$

First, note that the semi-norm $|\cdot|_{H^2}$ and the norm $\|\cdot\|_{H^2}$ are equivalent in $H^2_{\mathbf{n}_0}(\Omega)$ Quarteroni [2014], i.e, there exists $C_0 > 0$ such that $|u|_{H^2(\Omega)} \geq C_0\|u\|_{H^2(\Omega)}$, $\forall u \in H^2_{\mathbf{n}_0}(\Omega)$. Then, we have:

$$
\begin{aligned}
G(u, u) &= \underbrace{\mathbf{u}_n^t \mathbf{Q} \ \mathbf{u}_n}_{\geq 0} + \lambda \int_\Omega (\Delta u)^2 \\[2mm]
&\geq \lambda \int_\Omega (\Delta u)^2 = \lambda|u|_{H^2(\Omega)} \\[2mm]
&\geq \lambda C_0\|u\|_{H^2(\Omega)};
\end{aligned}
$$

hence, $G(\cdot, \cdot)$ is coercive.

We then show the continuity of $G(\cdot, \cdot)$. Since $H^2(\Omega) \subset C^0(\Omega)$ and since the norms $\|\cdot\|_\infty$ and $\|\cdot\|_2$ are equivalent on $\mathbb{R}^n$, there exists a constant C_1 such that $\|\mathbf{v}_n\|_\infty \leq C_2\|v\|_{H^2(\Omega)}$, $\forall v \in H^2(\Omega)$. Since $\mathbf{Q}$ is symmetric, its largest eigenvalue ρ is non negative. Then we have:

$$
\begin{aligned}
G(u, v) &= \mathbf{u}_n^t \mathbf{Q} \ \mathbf{v}_n + \lambda \int_\Omega (\Delta u)(\Delta v) \\[2mm]
&\leq \rho\|\mathbf{u}_n\|_\infty\|\mathbf{v}_n\|_\infty + \lambda|u|_{H^2(\Omega)}|v|_{H^2(\Omega)} \\[2mm]
&\leq \rho \, C_1^2\|u\|_{H^2(\Omega)}\|v\|_{H^2(\Omega)} + \lambda \, C_0^2 \ \|u\|_{H^2(\Omega)}\|v\|_{H^2(\Omega)} \\[2mm]
&\leq \max\left\{\rho \, C_1^2, \lambda \, C_0^2\right\}\|u\|_{H^2(\Omega)}\|v\|_{H^2(\Omega)}.
\end{aligned}
$$

And so the bilinear form $G(\cdot, \cdot)$ is also continuous. $\qquad\square$

We are now ready to give the proof of Proposition 4.1.

Proof. First of all, given $f \in H^2_{\mathbf{n}_0}$, the unique minimizer of the functional $\tilde{\mathcal{J}}_\lambda(\boldsymbol{\beta}, f)$ is given by:

$$\tilde{\boldsymbol{\beta}}(f) = (\mathbf{X}^t\mathbf{W}\mathbf{X})^{-1}\mathbf{X}^t\mathbf{W}(\mathbf{z} - \mathbf{f}_n). \tag{C.1}$$

To show that, we take the derivative of $\tilde{\mathcal{J}}_\lambda(\boldsymbol{\beta}, f)$ with respect to $\boldsymbol{\beta}$:

$$\frac{\partial \tilde{\mathcal{J}}_\lambda(\boldsymbol{\beta}, f)}{\partial \boldsymbol{\beta}} = -2\mathbf{X}^t \mathbf{W}(\mathbf{z} - \mathbf{f}_n) + (\mathbf{X}^t \mathbf{W} \mathbf{X})\boldsymbol{\beta}.$$

Since $\mathbf{X}$ is a full-rank matrix and $\mathbf{W}$ is invertible (the iith entry of $\mathbf{W}$ is in fact strictly positive, since it is different from zero and ≥ 0 by construction), $\mathbf{X}^t \mathbf{W} \mathbf{X}$ is invertible. Finally the necessary condition $\partial \tilde{\mathcal{J}}_\lambda(\tilde{\boldsymbol{\beta}}, f)/\partial \boldsymbol{\beta} = 0$ is satisfied if and only if $\tilde{\boldsymbol{\beta}}$ is given by (C.1). Since for fixed f, $\tilde{\mathcal{J}}_\lambda(\boldsymbol{\beta}, f)$ is clearly convex, $\tilde{\boldsymbol{\beta}}$ is a minimum.

Now, plugging $\tilde{\boldsymbol{\beta}}$ into the objective function, we obtain the following form of the functional:

$$\tilde{\mathcal{J}}_\lambda(f) = \mathbf{z}^t \mathbf{Q} \ \mathbf{z} - 2\mathbf{f}_n \mathbf{Q} \ \mathbf{z} + \mathbf{f}_n{}^t \mathbf{Q} \ \mathbf{f}_n + \lambda \int_\Omega (\Delta f)^2.$$

Since we want to optimize this functional with respect to f only, the problem becomes finding $\tilde{f} \in H^2_{\mathbf{n}_0}$ that minimizes:

$$\mathcal{J}_\lambda^*(f) = \mathbf{f}_n{}^t \mathbf{Q} \ \mathbf{f}_n + \lambda \int_\Omega (\Delta f)^2 - 2\mathbf{f}_n \mathbf{Q} \ \mathbf{z}. \qquad (\text{C.2})$$

We can then write $\mathcal{J}_\lambda^*(f) = G(f, f) - 2F(f)$, where

$$G(u, v) = \mathbf{u}_n^t \mathbf{Q} \ \mathbf{v}_n + \lambda \int_\Omega (\Delta u)(\Delta v) \qquad \text{and} \qquad F(v) = \mathbf{v}_n^t \mathbf{Q} \ \mathbf{z}.$$

Lemma C.1 ensures that $G(\cdot, \cdot)$ is a coercive and continuous bilinear form on $H^2_{\mathbf{n}_0} \times H^2_{\mathbf{n}_0}$; moreover, F is trivially a linear and continuous functional on $H^2_{\mathbf{n}_0}$. Applying the Lax-Milgram lemma and thanks to the symmetry of $G(\cdot, \cdot)$, the minimizer of the functional (C.2) is the function $\tilde{f} \in H^2_{\mathbf{n}_0}$ such that

$$\mathbf{u}_n^t \mathbf{Q} \ \tilde{\mathbf{f}}_n + \lambda \int_\Omega (\Delta u)(\Delta \tilde{f}) = \mathbf{u}_n^t \mathbf{Q} \ \mathbf{z}, \qquad \forall u \in H^2_{\mathbf{n}_0}$$

We conclude that $\tilde{f}$ exists and is unique and hence also $\tilde{\boldsymbol{\beta}}$ exists and is unique. $\qquad \square$

D   A general formulation of the model

We here present a unified formulation of the model, that comprehends as special cases the model versions for geostatistical and for areal data presented in the paper. Let $L : \mathcal{F} \to \mathbb{R}^n$ be a linear and continuous operator. Assume that $Y_1, \ldots, Y_n$ are independent, with Y_i having a distribution within the exponential family, with mean μ_i and common scale parameter ϕ. Let the mean vector $\boldsymbol{\mu}$ be defined by:

$$g(\boldsymbol{\mu}) = \boldsymbol{\theta} = \boldsymbol{X}\boldsymbol{\beta} + \mathbf{f}_n \qquad \text{where } \mathbf{f}_n = L(f).$$

We estimate $\boldsymbol{\beta} \in \mathbb{R}^q$ and the spatial field $f \in \mathcal{F}$ by maximizing the penalized log-likelihood functional in (2.2). We moreover define $\boldsymbol{\Psi}$ as the $n \times K$ matrix whose j−th column is given by $L(\psi_j)$, where ψ_j is the j−th finite element basis. If L is the linear operator that evaluates a function in $\mathcal{F}$ at n spatial locations $\mathbf{p}_1, \ldots, \mathbf{p}_n \in \Omega$, then $\mathbf{f}_n = (f(\mathbf{p}_1), \ldots, f(\mathbf{p}_n))^t$ and $\boldsymbol{\Psi}$ has the form in (4.4); we obtain in this case the model version for geostatistical data. If L is the linear operator that returns the integrals of a function in $\mathcal{F}$ over n disjoints subregions $D_1, \ldots, D_n$ of the domain Ω, then $\mathbf{f}_n = (\int_{D_1} f, \ldots, \int_{D_n} f)^t$ and the $n \times K$ matrix $\boldsymbol{\Psi}$ has entry (i, j) given by $\int_{D_i} \psi_j$; we obtain in this case the model version for areal data.

Owing to the linearity of the operator, the results presented in Sections 3 and 4 and in Appendices A, B and C carry over to the more general formulation of the model here presented, replacing the definition of $\mathbf{f}_n$ and $\boldsymbol{\Psi}$ with the more general definitions based on the linear operator L given above.
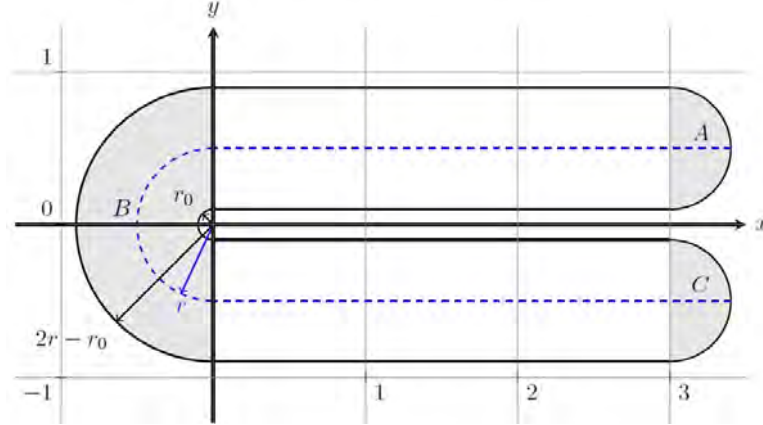
E   Test fields on horseshoe domain

Figure 10: Horseshoe domain used for the simulation studies of Section 6.

Figure 10 shows the Horseshoe domain used for the simulation studies of Section 6, where $q = \frac{\pi r}{2}$ and $\mathbf{1_A}(x, y)$, $\mathbf{1_B}(x, y)$ and $\mathbf{1_C}(x, y)$ are indicator functions defined as

$$\mathbf{1_A}(x, y) = \mathbf{1}_{\{(x-3)^2+(y-r)^2<(r-r_0)^2\}}(x, y)\mathbf{1}_{\{x>3\}}(x, y),$$
$$\mathbf{1_B}(x, y) = \mathbf{1}_{\{r_0^2 \le x^2+y^2 \le (2r-r_0)^2\}}(x, y),$$
$$\mathbf{1_C}(x, y) = \mathbf{1}_{\{(x-3)^2+(y+r)^2<(r-r_0)^2\}}(x, y)\mathbf{1}_{\{x>3\}}(x, y).$$

We set $r = 0.5$ and $r_0 = 0.1$.

The test field used for the simulation study with geostatistical data is defined as:

$$
f(x, y) = \begin{cases}
-\dfrac{1}{8} \left[x + q + (y - r)^2 + 10 \right] \mathbf{1_A}(x, y) & x > 3, \quad r_0 \le y \le 2r - r_0, \\[2ex]
-\dfrac{1}{8} \left[x + q + (y - r)^2 + 10 \right] & 0 \le x \le 3, \quad r_0 \le y \le 2r - r_0, \\[2ex]
\dfrac{1}{8} \left[\operatorname{atan}\left(\dfrac{y}{x}\right) r + (\sqrt{x^2 + y^2} - r)^2 + 10 \right] \mathbf{1_B}(x, y) & x < 0, \\[2ex]
-\dfrac{1}{8} \left[x + q + (y - r)^2 + 10 \right] & 0 \le x \le 3, \quad -r_0 \ge y \ge -2r + r_0, \\[2ex]
-\dfrac{1}{8} \left[x + q + (y - r)^2 + 10 \right] \mathbf{1_C}(x, y) & x > 3, \quad -r_0 \ge y \ge -2r + r_0.
\end{cases}
$$

The test field used for the simulation study with areal data is defined as:

$$
f(x, y) = \begin{cases}
\left[x + q + (y - r)^2 \right] \mathbf{1_A}(x, y) & x > 3, \quad r_0 \le y \le 2r - r_0, \\[2ex]
\left[x + q + (y - r)^2 \right] & 0 \le x \le 3, \quad r_0 \le y \le 2r - r_0, \\[2ex]
\left[-\operatorname{atan}\left(\dfrac{y}{x}\right) r + (\sqrt{x^2 + y^2} - r)^2 \right] \mathbf{1_B}(x, y) & x < 0, \\[2ex]
\left[-x - q + (y - r)^2 \right] & 0 \le x \le 3, \quad -r_0 \ge y \ge -2r + r_0, \\[2ex]
\left[-x - q + (y - r)^2 \right] \mathbf{1_C}(x, y) & x > 3, \quad -r_0 \ge y \ge -2r + r_0.
\end{cases}
$$

This is an affine transformation of the one considered for geostatistical data and coincides with the test function used in Wood et al. [2008].